Episodicity and Migration of Low Frequency Earthquakes modeled with Fast Fluid Pressure Transients in the Permeable Subduction Interface

Gaspard Farge[1*] Claude Jaupart[1] Nikolai M. Shapiro[2,3]

[1] Université de Paris, Institut de Physique du Globe de Paris, CNRS, F-75005 Paris, France
[2] Institut de Sciences de la Terre, Université Grenoble Alpes, CNRS (UMR5275), Grenoble, France
[3] Schmidt Institute of Physics of the Earth, Russian Academy of Sciences, Moscow, Russia

Manuscript submitted in Journal of Geophysical Research: Solid Earth, the 19^{th} February 2021.
This manuscript has not yet undergone peer-review, and will be subject to changes as it is reviewed. It will be regularly updated, and if accepted, the published version will be available via the "Peer-reviewed Publication DOI" link on this webpage.
Please feel free to contact the authors, feedback is welcome.

Abstract

In many subduction zones, the plate interface hosts intermittent, low-frequency, low-magnitude seismic tremor and low-frequency earthquakes (LFEs). Seismic activity clusters in episodic bursts that migrate along the fault zone in complex ways. Geological structures in fossil tremor source regions testify to large and pervasive variations of fluid pressure and permeability. Here, we explore the potential of fluid pressure transients in a permeable subduction interface to trigger seismic sources and induce interactions between them. We show how variations of pore pressure and permeability can act in tandem to generate tremor-like patterns. The core feature of the model is that low-permeability plugs behave as elementary fault-valves. In a mechanism akin to erosive bursts and deposition events documented in porous media, valve permeability opens and closes in response to the local fluid pressure distribution. The rapid pressure release and/or mechanical fracturing associated with valve opening acts as the source of an LFE-like event. Valves interact constructively, leading to realistic, tremor-like patterns: cascades, synchronized bursts and migrations of activity along the channel, on both short and long time and space scales. Our model predicts that the input fluid flux is a key control on activity occurrence and behavior. Depending on its value, the subduction interface can be seismically quiescent or active, and seismicity can be strongly time-clustered, quasi-periodic or almost random in time. This model allows new interpretations of low frequency seismic activity in terms of effective fluid flux and fault-zone permeability.

Plain language summary

During quiet periods between earthquakes, faults emit faint seismic signals, called tremor. Tremor seems to be emitted as the fault deforms slowly, channeling fluid at very high pressures from deep sources towards the surface. As such processes can both initiate or delay earthquakes on the fault, they are the subject of intense scrutiny. In this work, we build a simple model to explore how fluids flow within a subduction fault and how it can be linked to tremor. In our model, the fault's conduits sometimes clog, because the fluid that circulate in it carries particles. As the fluid brutally pushes its way through the plugs, it generates the seismic vibrations that we call tremor. We find that in geological conditions, the flow rate should be just right for a fault conduit to produce swarms of tremor which movements and behavior in time are very similar to typical observations of tremor. However, if the flux is either too low or too high, the fault should remain quiescent. Our model provides a framework to interpret seismic patterns as symptoms of how closed or open a fault is to fluid circulation, and how strong the fluid flux is within it.

*farge@ipgp.fr

This work was submitted to Journal of Geophysical Research: Solid Earth (19/02/2021)

Contents

This work was submitted to Journal of Geophysical Research: Solid Earth (19/02/2021)

1 Introduction

The extensive records of weak low-frequency seismicity that have been obtained in many fault zones over the last two decades provide powerful information on their dynamics. At intermediate depths (30–50 km) in several subduction zones, seismic activity takes the form of tremor [*e.g.*, 46, 55, 69, 71]. It now seems clear that these tremors are made of swarms of low-frequency earthquakes (LFEs) and many authors use the term tremor as a synonym for LFE activity [*e.g.*, 6, 19, 32, 33, 72, 77, 87, 91]. These LFEs appear to be due to repetitive, impulsive and localized sources [15, 33]. High rates of tremor activity are associated with geodetically observed slow deformation episodes called slow-slip events (SSEs) [*e.g.*, 27, 34, 57, 78]. The correlation between LFE and SSE activity gave rise to the term Episodic Tremor and Slip (ETS) [77]. In a more general acceptation, transient seismic and geodetic signals that are both generated during inter-seismic phases are often lumped together as *slow earthquake phenomena*. This new class of seismic and geodetic observations holds great promise for improving our understanding of the seismo-tectonic cycle.

According to the framework that prevails today, slow earthquakes are the "slow" analogs of "regular" earthquakes. Geodetic and seismic events are manifestations of the same process of slow slip at transitional depths in fault zones, in between unstable stick-slipping and stable sliding areas. The transitional part is made of slow sliding patches that are responsible for geodetic SSEs and that contain many small embedded frictionally unstable asperities generating LFEs. This framework explains why SSEs and tremor activity are correlated in time and accounts for the S-wave dominated LFE radiation pattern [*e.g.*, 88]. Numerical models of these phenomena [*e.g.*, 8, 13, 50, 60, 62, 89] are often based on the rate-and-state friction (RSF) formalism developed for "regular" earthquakes [29]. This efficient modeling approach has two significant shortcomings, however [96]. First, all the dynamic variability of the interface and its surroundings is collapsed on to a planar boundary. Second, it depends on empirical RSF parameters that are not inferred directly from processes occurring within the fault zone. Thus, it is difficult to specify RSF parameters and account for internal fault zone dynamics in a self-consistent manner. These shortcomings may be limiting in subduction zones because the brittle-to-ductile transition proceeds over an increasingly wide off-fault region as depth increases [73]. Source dimensions for tremor and LFEs are typically inferred to be a few hundred meters [*e.g.*, 23, 31, 92], close to the thickness of the highly deformed permeable fault zone [*e.g.*, 4]. This calls for more complete models dealing with processes in the interior of these zones.

There can be little doubt that pore fluid pressures and their variations play a key role in fault zone dynamics. From the frictional perspective, high pore pressures act to reduce the fault strength, bringing it closer to unstable sliding conditions. Numerous geophysical and geological observations provide evidence for fluid saturation in the subduction interface. It is widely believed that fluids are supplied by metamorphic dehydration reactions in the downgoing plate [37, 47, 64, 97]. High values of the V_p/V_s ratio and electrical conductivity indicate that pore fluids are at near-lithostatic pressures [6, 72, 98, among others], implying low values of fault strength. This explains why seismic activity is highly sensitive to very small dynamic stress changes generated by passing teleseismic waves [81] or tidal deformation [11, 79, 80, 95].

There is mounting evidence for large variations of pore pressure on the time scale of the slow-earthquake cycle. During slow slip events, seismic images, geodetic load studies as well as earthquake source mechanisms indicate that pore fluid pressures around the subduction interface drop markedly [42, 94, 99]. The migration of LFE activity is highly suggestive of pore-pressure diffusion [26, 35]. In exhumed subduction interfaces, one observes that the brittle-to-ductile transition is intrinsically coupled to transient pore-pressure cycling and fluid transport [4, 12, 73]. Episodes of fluid accumulation and drainage have been documented in shallow thrust faults and are recorded by metasomatic reactions in host rocks [3, 82, 93]. They have been attributed to changes of permeable pathways due to tectonic deformation, precipitation/dissolution or deposition/erosion processes [40, 53, 101].

With the recognition that pore fluid pressures are high and variable in the subduction interface, it may be misleading to attribute all geodetic and seismic events to slip to the exclusion of other processes. We argue that seismic tremor is likely due to very fast fluid pressure transients. Observations do not demonstrate unambiguously that slow slip events and low-frequency seismic radiation are both generated by the same process. It is true that these two types of activity are frequently correlated in time but a significant number of tremors and LFEs are recorded in the absence of detectable SSEs. Furthermore, the sources of seismic and geodetic events are not always co-located [*e.g.*, 57]. In addition, in some subduction zones, LFEs do not conform to the moment-duration scaling of classical shear rupture [20, 31]. One should finally note that the predominance of S-waves in the seismic signals does not necessarily establish a shear

This work was submitted to Journal of Geophysical Research: Solid Earth (19/02/2021)

rupture mechanism. S-wave dominated signals can arise from volumetric sources with non-spherical geometries [*e.g.*, 66] or from single-force sources associated with fast local pressure variations [85].

Strong arguments in favor of a fluid-related origin for LFEs comes from laboratory studies and volcano seismology. Laboratory experiments have established that tremor-like seismic activity can be caused by rapid post-failure fluid decompression [14]. In volcanic systems, shear deformation and slip do not play a predominant role, and yet tremors and LFEs (labelled as long-period earthquakes) are generated in abundance. These events have been attributed to fluid related processes [24]. In some cases, their sources are distributed over large depth intervals of a few tens of kilometers and appear to migrate on time scales of a few months or days [84]. These migrations have been attributed to pore-pressure transients associated with hydraulic connections between different parts of a volcanic plumbing system.

A key piece of information on fault zone dynamics is the distribution of LFEs in space and time. Here, we explore the potential of pressure transients in a permeable subduction interface to generate this type of activity. The structure and hydraulics of such a channel have rarely been studied in relation to seismicity [5, 26, 83, 102]. We investigate the behaviour of a heterogeneous channel containing plugs of low permeability. Pore pressure variations can arise in two different ways. First, through a time-dependent fluid supply, but there are no known mechanisms for strongly fluctuating rates of metamorphic dehydration reactions. Alternatively, one can invoke changes of permeability, as in the classical fault-valve model [90]. In this model, an increase of pore fluid pressure can generate an earthquake ruputure, which opens up or reactivates fluid pathways leading to an increase of permeability and a decrease of pore pressure. Clogging of pores due to precipitation from circulating fluids or to the trapping of particles then acts to decrease permeability, implying an increase of pore pressure and a new cycle of pressure change. The permeability increase of the first phase of the cycle can be achieved in two different ways. One is shear displacement in association with fault dilation [52] — although it appears that, in some cases, this may in fact act to decrease permeability in the slip direction [7]. In the other mechanism, high fluid pressures induce fracturing and/or unclogging of small pores and pore throats. Impulsive flushing events have been observed in a variety of settings and have been called *erosive bursts* [16, 54]. In this framework, mechanical forces caused by fast local pore pressure variations [85] and/or rupture of brittle heterogeneities [30, 58] may be responsible for LFEs. One expects that the unclogging of an individual plug induces a rapid pore pressure drop that propagates to neighbouring plugs and generates swarms of similar events.

The paper is organized as follows. We first describe the main characteristics of tremor/LFE activity in subduction zones that must be accounted for by any physical model. We then develop a quantitative model, starting with the basic processes that are involved and the corresponding equations. Results are described for a range of fluid input rates and a regime diagram is obtained and justified by simple theoretical arguments. The activity patterns that are generated are compared to observed ones, and conditions that must be met for a successful model are discussed.

2 Tremor patterns observed in subduction zones

We summarize the most salient features of tremor activity in subduction zones. The Guerrero, Mexico, area is particularly appropriate for studies of LFE migration because it stretches over a lateral distance of more than 100 km in association with a small subduction angle. A very large catalog of events is available there [33].

2.1 Spatial Segmentation

At a local scale, the fact that LFEs occur in families of recurring events with similar waveforms indicates that they are due to the repeated activation of individual sub-kilometric scale sources [23]. In subduction zones, activity is often segmented in the along strike direction and concentrated in patches [21, 74]. In Shikoku, Japan, and elsewhere, events delineate pluri-kilometric striations that are aligned with the subduction direction and that have been linked to the subduction of seamount chains [48]. Shorter striations have also been observed in the Olympic Peninsula, Cascadia [39]. In Guerrero, Mexico, activity is split into two well-separated patches along the dip of the interface [33, 46, 57, 71] (Figure 1).

2.2 Tremor Migration

Bursts of tremor activity migrate along the subduction interface on time scales of seconds to weeks, and space scales from a few to a few hundreds of kilometers. Short-lived short-distance migrations are

This work was submitted to Journal of Geophysical Research: Solid Earth (19/02/2021)

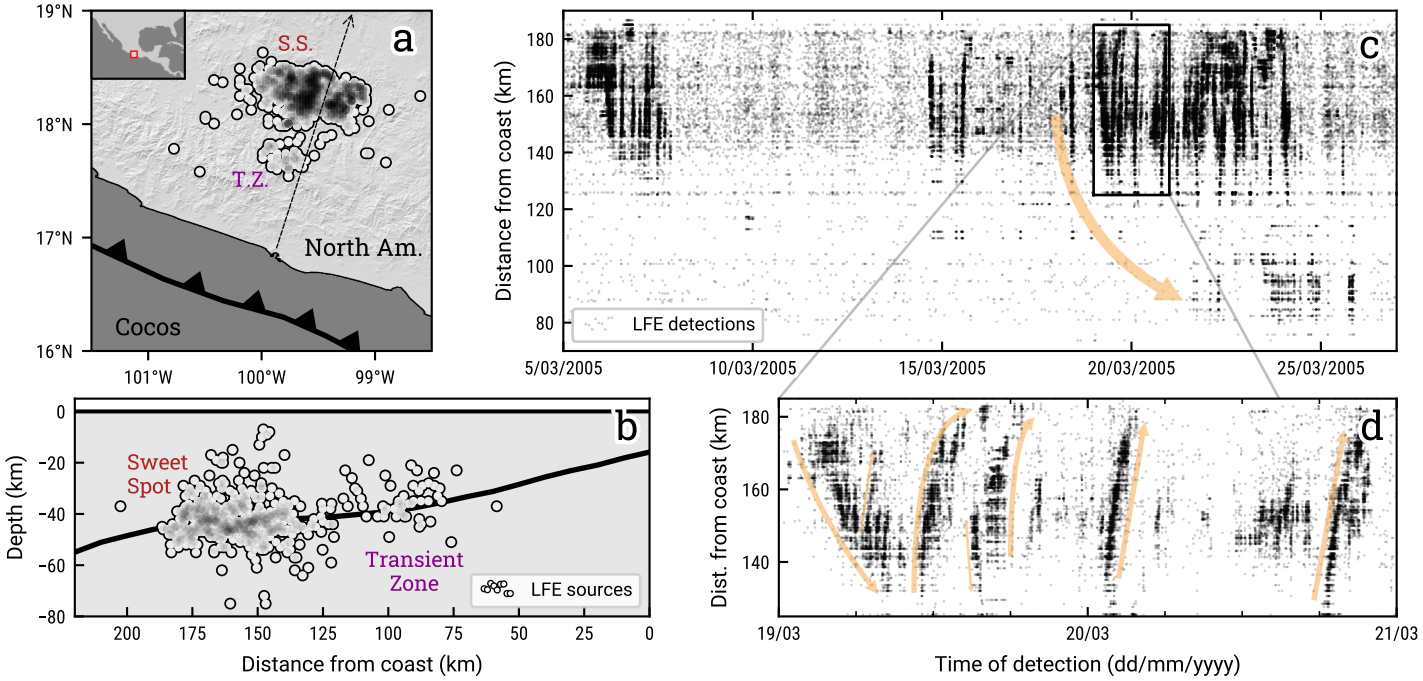

Figure 1: The Guerrero (Mexico) tremor zone in map view *(a)* and vertical cross-section *(b)*. Thick black lines outline the trench and the subduction interface (data from [43]). *(c)* and *(d)*, LFE activity in a time-location chart from the [33] catalog. Activity occurs in two patches centered on the subductioon interface, a dense downdip one called the *sweet spot* and a sparser updip one called the *transient zone*. Tremor activity migrates along the subduction interface in both the updip and downdip directions, as shown by the orange arrows.

often restricted to an individual tremor patch and proceed at rates in a 10–100 km/hr range (on time scales T of minutes to hours over length scales L of tens of kilometers) [26, 39]. In marked contrast, long-lived, long-distance migrations that connect spatially separated patches are slower with velocities in a $\sim$ 1–10 km/day range ($T \sim$ weeks to months, $L \sim 100$ km) [35, 56]. Such systematics between time and space scales are reminiscent of a diffusion process.

In Japan and Cascadia, the largest transients of activity ($T \sim$weeks, $L \sim$100 km) propagate along strike in a belt lying in a 30 to 60 km depth range. This led to the idea that this depth interval delineates the zone rheologically able to enable slow-slip [41, 49]. In Guerrero, the downgoing plate geometry allows for a very long part of subduction interface to remain at tremor prone depths and it is clear that the largest migrations systematically originate from the deep end of the fault and slowly propagate updip [35].

Short-lived migrations ($T \sim$ minutes to hours) often proceed along striations [49], sometimes in rapid sweeps [39]. Remarkably, these rapid migrations sometimes occur within larger scale migrations, propagating in the reverse direction with respect to the large scale propagation. This has been observed in the along dip direction in Guerrero, Mexico [26, 33] and in the along strike direction in Cascadia [44].

2.3 Temporal Patterns

Tremor activity occurs during episodic *bursts* of events, which are in themselves composed of shorter bursts. time clustering of activity covers time scales of years for the largest bursts — often correlated with slow-slip events and long-distance migrations – to days or even minutes for smaller bursts [51, 100] — called *cascades*. These occur over an apparent duration that depends on the scale of observation [33, 86]. As a temporal point process, this activity does not conform to simple memoryless realizations and has been described using non-Poissonian statistics [9, 36].

The recurrence interval between tremor bursts decreases — in other words activity evolves from episodic to highly clustered in time — with increasing depth along the subduction interface [100]. Within an individual tremor patch, the level of time clustering does not remain constant in time, providing evidence for changing conditions in the fault zone [36].

This work was submitted to Journal of Geophysical Research: Solid Earth (19/02/2021)

2.4 Tremor activity Patterns in Guerrero, Mexico

Figure 1 shows the spatio-temporal patterns of LFE activity in the Guerrero tremor subduction segment, which is concentrated in two separate patches. One, called *sweet spot*, is located at the downdip end of the segment and has a high rate of activity with a high level of time clustering [36]. The other patch, called *transient zone* [33], is further updip and on the whole more quiescent. It hosts episodic bursts of activity with a recurrence interval of about 3 months [33], which coincide with short-term SSEs recurrence [34]. One of these episodes is displayed in Figure 1c. It migrates over a hundred kilometers updip, away from the sweet spot. These episodes are built from many shorter bursts that may migrate in both updip and downdip directions (Figure 1c).

The Guerrero subduction zone is known for its very large SSEs that recur at intervals of about 4 years [*e.g.*, 76]. These events persist for several months with slow slip occuring mostly updip of the tremor-generating region. The slow-slipping segment lies completely out of the sweet spot, and encroaches on the transient zone at its downdip end, where short-term SSEs are concentrated. Timewise, there is a significant correlation between large SSEs and tremor intensification in both the sweet spot and the transient zone [46]. At the times of large SSEs, tremor activity in the transient zone switches from episodic to highly clustered [36]. These systematics suggest that SSEs and tremor are both related to the same physical process. However, the fact that patches with maximum tremor activity (the sweet spot) and with the largest amount of slow slip (the transient zone) are separated by more than 50 km does not seem consistent with the hypothesis in which tremor originates solely from slip processes. One solution is to introduce a complex distribution of rheological properties or RSF parameters in the fault zone. An alternative solution, which is pursued here, is to invoke hydraulic transients in a heterogeneous permeable subduction interface.

3 Model design

In this section, we develop a model for time changes of permeability in a heterogeneous porous channel that runs along the dip of the subduction interface.

3.1 Diffusion equation for pore pressure variations

Pore connectivity is modeled at a macroscopic level with a permeability that varies along the channel $k(x)$. The fluid mass flux per unit cross-sectional area, $q(x,t)$, depends on pore pressure $P(x,t)$ according to Darcy's law:

$$q(x,t) = -\frac{k(x)\rho}{\eta}\left(\frac{\partial P}{\partial x}(x,t) + \rho g \sin\alpha\right) \tag{1}$$

where ρ is the fluid's density, η is the fluid viscosity, α is the dip angle of the subduction interface and g the acceleration of gravity. Mass balance dictates that :

$$-\frac{\partial q}{\partial x}(x,t) = \frac{\partial(\rho\phi)}{\partial t}. \tag{2}$$

where ϕ is porosity. We consider that pores are saturated with fluid and neglect temperature changes, which is justified by the small thickness of the channel and the small flow rates that are expected. Changes of the local mass of fluid can be due to the fluid compressibility as well as expanding/contracting pores. This is accounted for by an effective compressibility noted β, such that:

$$\begin{aligned} \beta &= \frac{1}{\rho\phi}\frac{\partial(\rho\phi)}{\partial P} \\ \implies -\frac{\partial q}{\partial x}(x,t) &= \rho\phi\beta\frac{\partial P}{\partial t}(x,t). \end{aligned} \tag{3}$$

For simplicity, we neglect density variations in the body force term in equation (1), because they are due to changes of flow-induced dynamic pressure, which account for a fraction of the total pressure, and because they are not expected to play a significant role. We split pressure into a hydrostatic component and a time-dependent dynamic component due to flow noted p. Neglecting changes of fluid viscosity, we obtain the following equation for the dynamic pore pressure component:

This work was submitted to Journal of Geophysical Research: Solid Earth (19/02/2021)

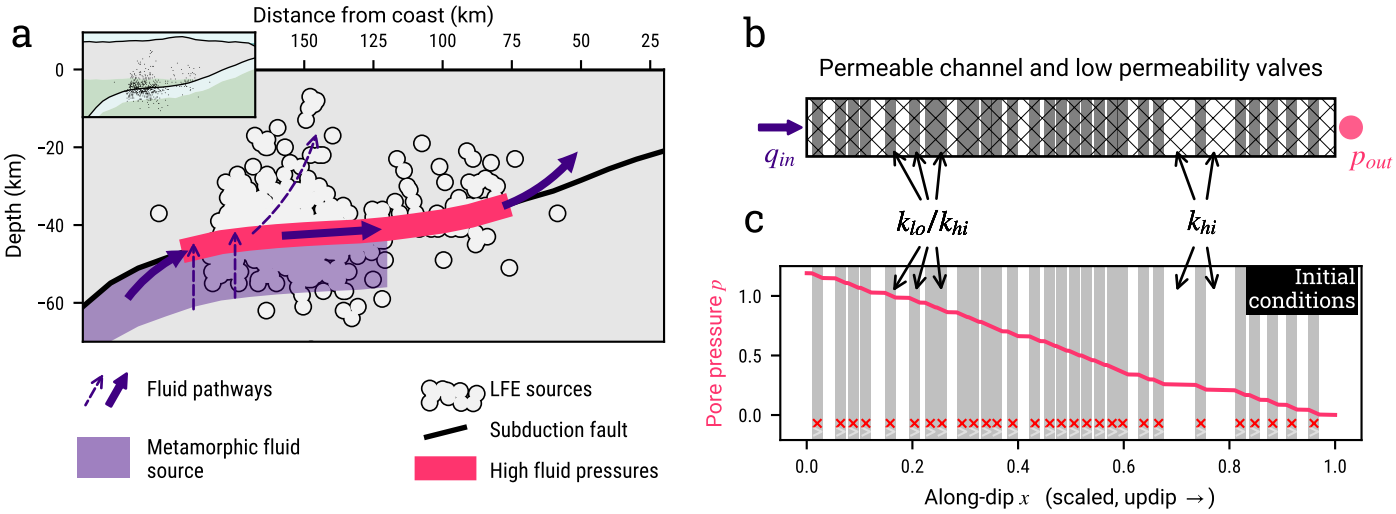

Figure 2: *(a)* Schematic representation of a permeable fault zone. Below the tremor source region, metamorphic dehydration reactions release fluid, which is channeled in the permeable subduction interface as it circulates under high fluid pressures. *(b)* Permeability structure for a 1-D hydraulic model of this system, involving a number of randomly distributed plugs that can open and close under certain conditions. The channel is fed at its base by input fluid flux q_{in}. At the top, the channel is connected to a high permeability region such that the fluid pressure is close to the hydrostatic pressure p_{out}. *(c)* Initial conditions correspond to steady-state flow regime with a small input flux and all plugs closed.

$$\frac{\partial p}{\partial t} = \frac{1}{\phi\beta\eta}\frac{\partial}{\partial x}\left(k(x)\frac{\partial p}{\partial x}\right). \tag{4}$$

We shall assume that permeability is piecewise constant. Thus, in each segment, the dynamic pressure obeys a diffusion equation:

$$\frac{\partial p}{\partial t} = \frac{k}{\phi\beta\eta}\frac{\partial^2 p}{\partial x^2}\ . \tag{5}$$

with diffusivity $D = k/(\phi\beta\eta)$. Along the modeled channel, D is therefore piecewise constant.

3.2 A mechanism for large changes of permeability

Our model has two main ingredients, which deal with the nature of the fluid phase and its interaction with the network of pores in the permeable medium. Subduction zone metamorphic fluids are complex silica-saturated mixtures [37, 64]. As they rise, they undergo decompression and, due to the pressure dependence of solubility, are expected to precipitate either amorphous silica (silica gel) or quartz nanoparticles as well as other mineral phases. Depending on the availability of nucleation sites, precipitation may proceed along the pore walls or in the bulk fluid. High temperature decompression experiments on silica-rich fluids demonstrate that the silica nanoparticles that are generated are readily mobilized by fluid flow [2, 70]. Small clasts generated by grinding motion along the fault are also likely involved. Thus, as in other deep permeable systems, the interstitial fluid phase is expected to carry fines and colloids [63].

In a majority of natural situations, the permeable medium is made of pores and fractures connected by thinner throats. Capture and/or precipitation of even small amounts of solids within throats can decrease permeability by orders of magnitude [65]. Calculations by [10] show that, depending on whether pore throats are open or clogged, permeability can change by more than a factor of ten. These changes are associated with negligible porosity variations because pore throats occupy a very small fraction of the total interstitial volume. Thus, the transition between high and low permeability states is very abrupt. Even if they are much smaller than a pore throat, fines and colloids can get stuck through a jamming process at rates that depend on their concentration [1, 25, 28]. Clogging can be achieved in a matter of minutes [22, 28, 63].

This work was submitted to Journal of Geophysical Research: Solid Earth (19/02/2021)

Material that gets stuck in pore throats may get remobilized by the fluid [17, 25, 54, 59]. Flow exerts a shear stress on the encasing solid, noted σ, that scales with $d(\partial p/\partial x)$, where d is the average pathway diameter. If this stress exceeds a certain threshold value noted σ_c, infillings are eroded and transported by the fluid [25]. This may occur in catastrophic fashion in events called *erosive bursts* [16, 68]. Such bursts may be composites of several smaller unclogging events [16, 68]. As long as $\sigma > \sigma_c$, particles cannot remain stuck and incipient coatings of pore walls are eroded, ensuring that fluid pathways stay fully open. Thus, clogging requires that $\sigma \leq \sigma_c$. The gradual clogging of pathways is therefore hampered by the unclogging events that keep recurring. Because of this intermittence beween erosion and deposition regimes, particles and colloids do not get permanently cemented to one another and to pore walls. Clogging and unclogging events proceed rapidly, on the scale of hours to days, and will be considered as instantaneous at the time-scales of LFE activity.

3.3 A valve mechanism

We model clogging and unclogging events as follows. Within a long permeable channel, let us consider a clogged plug where fluid pathways are narrow and contorted because they wrap around captured particles (closed state). In this case, the average pathway aperture d and permeability k are both small, with values d_{lo} and k_{lo}, respectively. If and when δp, the pressure difference across the plug, reaches a critical value noted δp_c^{break} such that the wall shear stress σ is equal to critical value σ_c, the plug breaks and unclogging occurs. As a consequence, pore throats are no longer obstructed by particles and permeability increases to $k_{hi} \gg k_{lo}$, in association with an increase of d from d_{lo} to d_{hi} (open state). Note that, as mentioned above, porosity is barely affected because pore throats account for a very small fraction of the total interstitial volume. This drives a lowering of pore pressures upstream of the plug, and an increase downstream. This pressure transient proceeds initially very rapidly and then at decreasing rates in a diffusion-induced flow transient. A key point is that σ initially increases. Just before unclogging, it is equal to:

$$\sigma_- = \lambda_1 d_{lo} \frac{\delta p_c^{break}}{w} = \sigma_c \tag{6}$$

where λ_1 is a coefficient and w is the plug length along the channel. As D increases from d_{lo} to d_{hi}, σ increases to σ_+:

$$\sigma_+ = \lambda_1 d_{hi} \frac{\delta p_c^{break}}{w} \tag{7}$$

which is larger than σ_c. σ then decreases gradually as the pressure distribution adapts to the new permeability structure. The plug remains unobstructed as long as σ is larger than σ_c. Clogging occurs when $\sigma = \sigma_c$ such that δp reaches a second threshold value noted δp_c^{clog}:

$$\lambda_1 d_{hi} \frac{\delta p_c^{clog}}{w} = \sigma_c \tag{8}$$

Clogging causes the permeability to drop back to k_{lo}, driving an increase in δp until unclogging occurs again, thus starting a new cycle. This is a valve behaviour akin to the toggle-switch of [67].

This framework allows an internally consistent mechanism for a succession of unclogging and clogging events. One requirement is that $\delta p_c^{clog} < \delta p_c^{break}$. From equations (6) and (8), we deduce that:

$$\frac{\delta p_c^{break}}{\delta p_c^{clog}} = \frac{d_{hi}}{d_{lo}}. \tag{9}$$

Thus, the fact that $d_{hi} > d_{lo}$ automatically ensures that $\delta p_c^{clog} < \delta p_c^{break}$. One can go one step further using relationships between the average width of fluid pathways d and permeability k. A common parameterization is the Kozeny-Carman equation [25]:

$$k = \lambda_2 \frac{\phi d^2}{\tau} \tag{10}$$

where λ_2 is a coefficient that depends on the nature of the fluid pathways, *e.g.* tubes or slits, ϕ is porosity and τ is tortuosity. We may neglect variations of porosity, as discussed above, and obtain:

$$\frac{k_{hi}}{k_{lo}} = \frac{\tau_{closed}}{\tau_{open}} \left(\frac{d_{hi}}{d_{lo}} \right)^2 \tag{11}$$

This work was submitted to Journal of Geophysical Research: Solid Earth (19/02/2021)

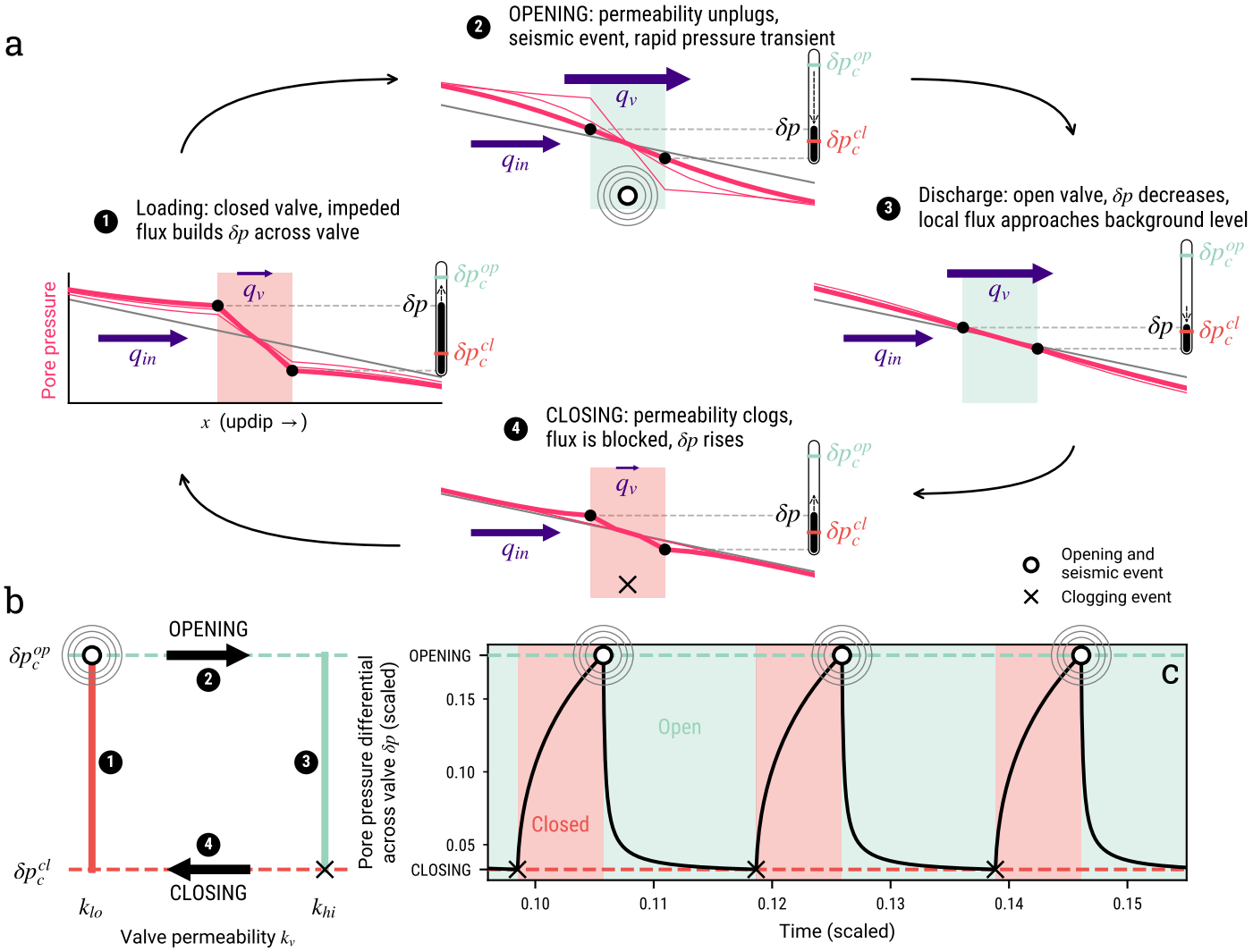

Figure 3: *(a)* The 4 stages of the valve mechanism. *1*, the valve has been closed and permeability is k_{lo}. δp, the pressure difference across the valve, increases. *2*, when δp reaches the threshold value δp_c^{break}, an impulsive unclogging event (an erosive burst) occurs. Particles get flushed out, the valve opens and permeability rises to k_{hi}. *3*, valve opening generates a rapid pressure transient that is associated with a low frequency earthquake. *4*, when δp decreases to δp_c^{clog}, the deposition of fines and colloids resumes and permeability drops to k_{lo}. The valve closes and a new cycle begins. *(b)* Hysteretical cycle of pressure difference δp and valve permeability k. *(c)*. Evolution of δp through 3 successive cycles of valve opening and closure for an isolated valve.

where τ_{open} and τ_{closed} are the tortuosities of the open and closed plugs. Fluid pathways are more irregular and contorted in a closed plug than in an open one, implying that $\tau_{closed} > \tau_{open}$. Using equation (9, one deduces that:

$$\frac{\delta p_c^{break}}{\delta p_c^{clog}} = \frac{d_{hi}}{d_{lo}} = \left(\frac{\tau_{open}}{\tau_{closed}} \frac{k_{hi}}{k_{lo}} \right)^{1/2} \tag{12}$$

For the small porosity media that are involved here, tortuosity ratio $\tau_{open}/\tau_{closed}$ is likely to be in a $1/2 - 1/4$ range [38]. As stated above, permeability changes induced by clogging are typically larger than one order of magnitude [10, 65], which guarantees that $\delta p_c^{break} > \delta p_c^{clog}$. For the sake of further discussion in section 4.1, it should be noted that such values of tortuosity ratio imply that $k_{hi}/k_{lo} > \delta p_c^{break}/\delta p_c^{clog}$.

This work was submitted to Journal of Geophysical Research: Solid Earth (19/02/2021)

3.4 Valves as elementary seismic sources

Plugs that open and close act as valves. The sudden fluid pressure transient that accompanies the opening of a valve generates an impulsive force on the solid matrix. We also note that the buildup of pore pressures that eventually leads to unclogging may also induce fracturing. Thus, following [85], we consider that as they open, valves act as elementary seismic sources and generate LFE-like events.

3.5 Permeability values, boundary and initial conditions

We shall consider a heterogeneous permeable channel with a series of randomly distributed valves. This corresponds to one type of random permeability distribution involving segments where fluid pathways are more contorted than elsewhere. The behaviour of any valve depends on what happens in neighbouring ones, so that pressures and flow rates must be calculated everywhere in the channel.

Metamorphic reactions occur at different depths depending on the dehydrating material, which includes sediments, serpentinized mantle and hydrated oceanic crust. Focussing on the oceanic crust, dehydration proceeds at depths exceeding the tremor source region [97] and most of this fluid gets trapped in the high permeability subduction interface, sealed from above by the low permeability mantle wedge [47]. Thus, the channel is fed at its base by fluid flux q_{in}. For a first instalment of the model, it is instructive to maintain this flux at a constant value. At its top, the channel is connected to a high permeability region which may be either continental crust [47] or an accretionary prism. In this case, pore pressures are close to hydrostatic values, such that the dynamic pressure is zero ($p_{out} = 0$).

For simplicity, we shall assume that in the channel outside of valves, permeability remains constant at the value k_{hi} and that valves have the same length w in the x direction. Physical variables are made dimensionless using scales described in Table 1. Values adopted for the various valve parameters are listed in Table 2. Boundary and initial conditions are illustrated in Figure 2b,c. We start all simulations with an equilibrium profile corresponding to a low value of flux $q_{in}(t < 0) = 0.09$, such that all valves are closed with permeability k_{lo}. At $t = 0$, q_{in} is changed to its definitive value.

Table 1: Characteristic dimensions used to scale physical variables

Variable		Characteristic scale	
x	Distance along channel	$\mathcal{X} = L$	Channel length
z	Depth	$\mathcal{Z} = \mathcal{X}\sin(\alpha)$	Channel vertical depth
t	Time	$\mathcal{T} = \mathcal{X}^2/D$	Diffusive time[a]
p	Pore pressure	$\mathcal{P} = (\rho_r - \rho)g\mathcal{Z}$	Reduced lithostatic pressure differential across channel
q	Massic flow rate[b]	$\mathcal{Q} = k_{hi}\rho/\eta \times \mathcal{P}/\mathcal{X}$	Flux resulting from characteristic pore pressure differential[a]
k	Permeability	$\mathcal{K} = k_{hi}$	Background channel permeability

[a] along a fully open channel, $D = k_{hi}/(\rho\eta\beta)$
[b] per unit channel cross section area

Table 2: Valve parameters for all simulations presented in this study

Parameter		Value (scaled)
w	Valve width	0.02
k_{hi}	Open valve permeability	1
k_{lo}	Closed valve permeability	0.05
δp_c^{break}	Threshold p difference for opening	0.04
δp_c^{clog}	Threshold p difference for closing	0.021
q_c^{break}	Flux above which a closed valve can open	0.1
q_c^{clog}	Flux below which an open valve can close	1.05

3.6 Numerical implementation

Solutions for the pressure field in time were obtained using a Crank-Nicholson finite difference scheme, with a first order, centered discretization of the second order space derivatives of pressure [75, section

This work was submitted to Journal of Geophysical Research: Solid Earth (19/02/2021)

20.2, pp 1045–1048]. The scheme is implicit, centered and second order in time, and is unconditionnally stable. Valves are either in an open or a closed state, as described in section 3.3 above, and when the pressure differential at their boundary reaches a threshold value, their open/close state is changed accordingly. Each opening of a valve is counted as a seismic event.

In all simulations presented here, distance along the fault is discretized in dimensionless increments $\delta x = 0.002$ and the dimensionless time step is set to $\delta t = h^2/2D = 2.10^{-6}$. In order to test the accuracy of the numerical implementation, we calculated analytically the pressure variations that follow an unclogging event in and around an isolated valve, and compared them to numerical solutions. Convergence was then tested by lowering both space and time steps, and we verified that accuracy improved with increasingly fine discretization.

4 Time-dependent valve behaviour

We first use a single valve to show how the activity regime is controlled by the input flux and how an intermittent open and closed behavior requires certain conditions (Figure 5). We then illustrate the valve-to-valve interaction process using 3 valves (Figure 6).

4.1 A single valve

As mentioned above, the valve mechanism depends on five control parameters, four that describe valve behaviour, $k_{lo}, k_{hi}, \delta p_c^{clog}, \delta p_c^{break}$, and the input flux q_{in}. We identify the conditions under which a steady state solution exists, with a valve that is either open or closed. One has:

$$q_{in} = \frac{\rho}{\eta} k_v \frac{\delta p}{w}. \tag{13}$$

where k_v, the valve permeability, may be equal to k_{lo} or k_{hi}, and where δp is again the pressure difference across the valve. If $\delta p \leq \delta p_c^{break}$ in a closed valve, stuck particles cannot be removed and the valve remains closed. Conversely, if $\delta p \geq \delta p_c^{clog}$ in an open valve, particles cannot be captured and the valve remains open. These conditions can be expressed as follows, using q_{in}, the flux valve is subject to:

$$q_{in} \leq \frac{\rho}{\eta} k_{lo} \frac{\delta p_c^{break}}{w} \; (= q_c^{break}) \text{ for a closed valve,} \tag{14}$$

$$q_{in} \geq \frac{\rho}{\eta} k_{hi} \frac{\delta p_c^{clog}}{w} \; (= q_c^{clog}) \text{ for an open valve.} \tag{15}$$

which introduces two threshold values for the fluid flux, noted q_c^{break} and q_c^{clog}, respectively. The two conditions in (14) and (15) define domains in $(\delta p, k_v)$ space corresponding to a closed valve or an open one in steady-state (Figure 4). Table 2 lists values for the pressure thresholds and permeabilities, as well as for the flux thresholds used for the valve set up of this study.

Depending on the four valve parameters, there are two different types of solutions. Let us first consider *enhanced permeability variations*, such that $k_{hi}/k_{lo} > \delta p_c^{break}/\delta p_c^{clog}$. In this case, $q_c^{break} < q_c^{clog}$ and there are no steady-state solutions in the $q_c^{break} - q_c^{clog}$ interval (Figure 4a). In this interval, the input flux being higher than q_c^{break}, a closed valve will open, and in turn, the input flux being lower than q_c^{clog}, the now open valve will close eventually. Therefore, the valve must constantly switch between open and closed states in order to handle the imposed input flux. This oscillatory regime is illustrated schematically in Figure 3.

In the other case, called *enhanced pressure variations*, $k_{hi}/k_{lo} < \delta p_c^{break}/\delta p_c^{clog}$. This implies that $q_c^{break} > q_c^{clog}$ and the domains for a closed valve and an open one overlap in the $q_c^{clog} - q_c^{break}$ interval. In this interval, steady-state solutions are possible for the two valve states (Figure 4b). Which one is selected depends on the initial state of the valve. In this case, therefore, there no valve activity.

This analysis leads to the following instability criterion for the valve:

$$q_c^{clog} < q_c^{break} \iff \frac{\delta p_c^{break}}{\delta p_c^{clog}} < \frac{k_{hi}}{k_{lo}}. \tag{16}$$

In a geological context, the tortuosity ratio is small and lies in a restricted range (see above) and permeability is expected to change by one order of magnitude [10, 65, 67]. Using equation (12) derived above for the threshold δp ratio, we conclude that the instability criterion should be met in geological

This work was submitted to Journal of Geophysical Research: Solid Earth (19/02/2021)

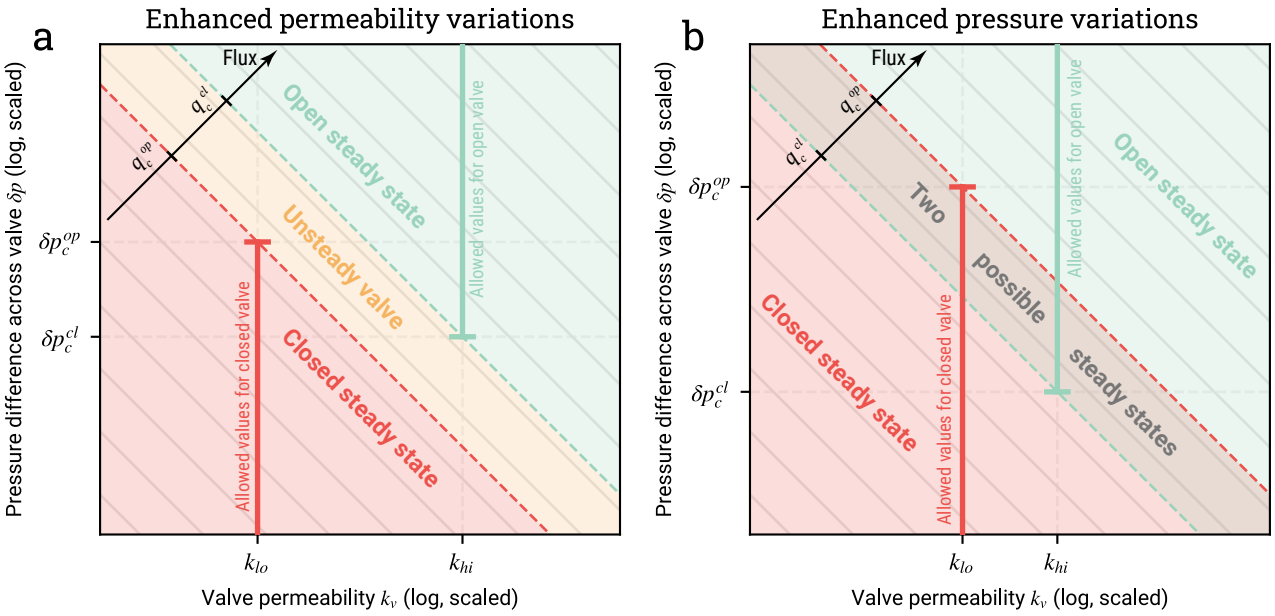

Figure 4: Requirements for steady-state valve regimes (equations (14) and (15)) in k-δp space (in log-log scale). The two values for permeability k and threshold values for the valve pressure difference δp are shown with vertical and horizontal dashed lines. In this space, iso-flux contours appear in gray lines of slope -1 in log-log scale (-45^o). Blue and red segments indicate values of δp that are allowed for a closed valve and an open one in steady-state, respectively. Steady-state conditions are achieved in the green and red shaded areas. See explanations in the text. *(a)* Valve with enhanced permeability variations ($k_{hi}/k_{lo} > \delta p_c^{break}/\delta p_c^{clog}$). *(b)* Valve with enhanced pressure variations ($k_{hi}/k_{lo} < \delta p_c^{break}/\delta p_c^{clog}$).

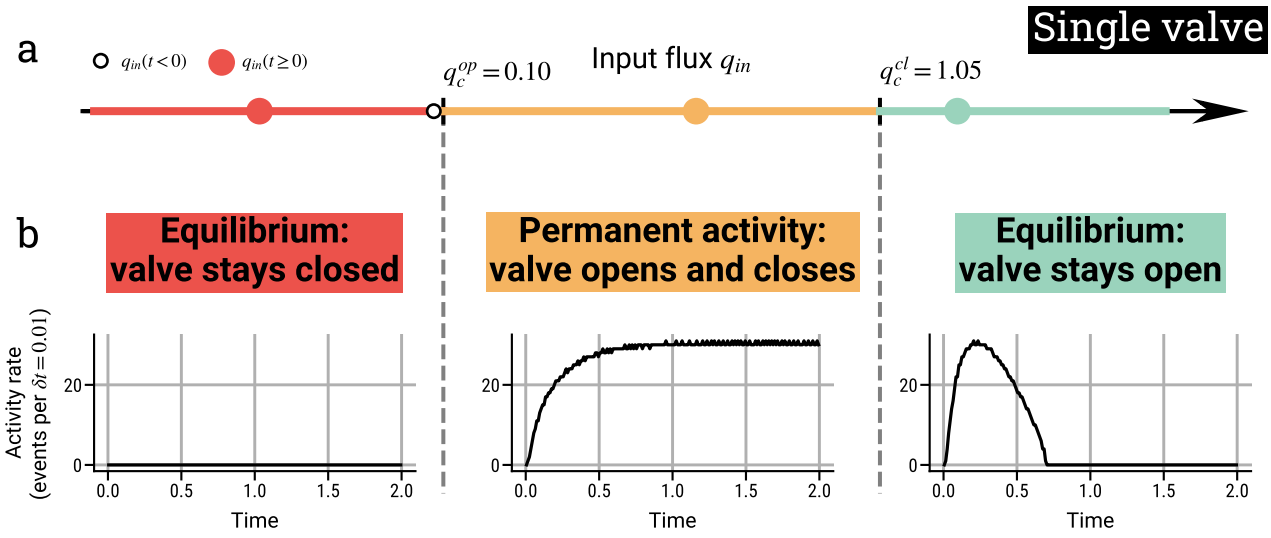

Figure 5: Influence of the input flux q_{in} on the activity of a single valve. *(a)* Three intervals of input flux q_{in} are delimited by two threshold values q_c^{clog} and q_c^{break}. *(b)* Examples of activity rate evolution in time (in black) for each regime. Activity rate is taken as the number of events per $\delta t = 0.01$, scaled unit. An event corresponds to the opening of a valve.

This work was submitted to Journal of Geophysical Research: Solid Earth (19/02/2021)

context. Figure 5 shows results for three values of input flux, corresponding to steady-state with a closed valve ($q_{red} < q_c^{clog}$), unstable valve that switches between closed and open states ($q_c^{clog} < q_{yellow} < q_c^{break}$), and finally steady-state with an open valve ($q_{green} > q_c^{break}$). In the first case, q_{red} is too low to allow the valve to open at all, no activity is recorded. In the last case, q_{green} is so high that after an initial transient during which the valve opens and closes to accomodate the incoming flux, the valve ends up open, submitted to a flux that does not allow it to close. In the intermediate case, q_{yellow} is both high and low enough to allow the valve to open when closed, and to close when open. After an initial transient, the valve activates in a very regular fashion.

4.2 Valve-valve interaction via pore pressure diffusion

A simulation with three valves shows that how the opening of a valve may trigger the opening of adjacent valves (Figure 6). In this simulation, the middle valve *v2* opens up, driving a sudden permeability increase. As a consequence, the δp that has built up across the valve re-equilibrates through diffusion, decreasing pressure updip of the valve and increasing it downdip of it. This induces an increase of pore pressure gradient through the two adjacent valves, eventually bringing them closer to unclogging conditions. We note that such constructive interaction may cause migrations of activity in cascades, in both up- and downdip directions.

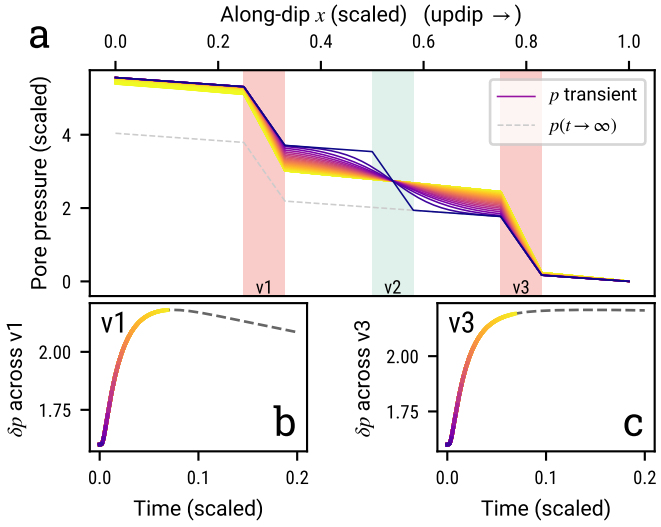

Figure 6: Interactions between three neighbouring valves. *(a)* Transient evolution of pore pressure from an initial equilibrium profile with all valves closed towards a profile with valves *v1* and *v3* closed and valve *v2* open. Panels *(b)* and *(c)*: pore pressure difference evolution across valves *v1* and *v3*.

5 Emergence of collective behavior patterns for a large number of interacting valves

We now explore systematically a model involving 29 randomly distributed valves (Figure 2b). All the valves are identical, we take the same permeability and threshold δp as before, implying that the threshold flux q_c^{clog} and q_c^{break} are the same (equations (14) and (15), Table 2). We focus on enhanced permeability variations conditions because they are relevant for fault zones. As for a single valve, there are three permanent regimes in which this system can be. One with intermittent valve activity and two quiescent ones (Figure 9).

Model outputs for runs with low ($q_{in} = 0.16$) and high ($q_{in} = 0.81$) input fluxes are shown in Figure 7 and Figure 8. At any given time, a simple diagnosis of the state of the system is given by the bulk equivalent permeability k_{eq}. Considering that channel segments and open and closed valves constitute hydraulic resistors in series, k_{eq} can be written:

$$k_{eq} = \frac{L}{(L - N_{cl}w)/k_{hi} + N_{cl}w/k_{lo}} \tag{17}$$

This work was submitted to Journal of Geophysical Research: Solid Earth (19/02/2021)

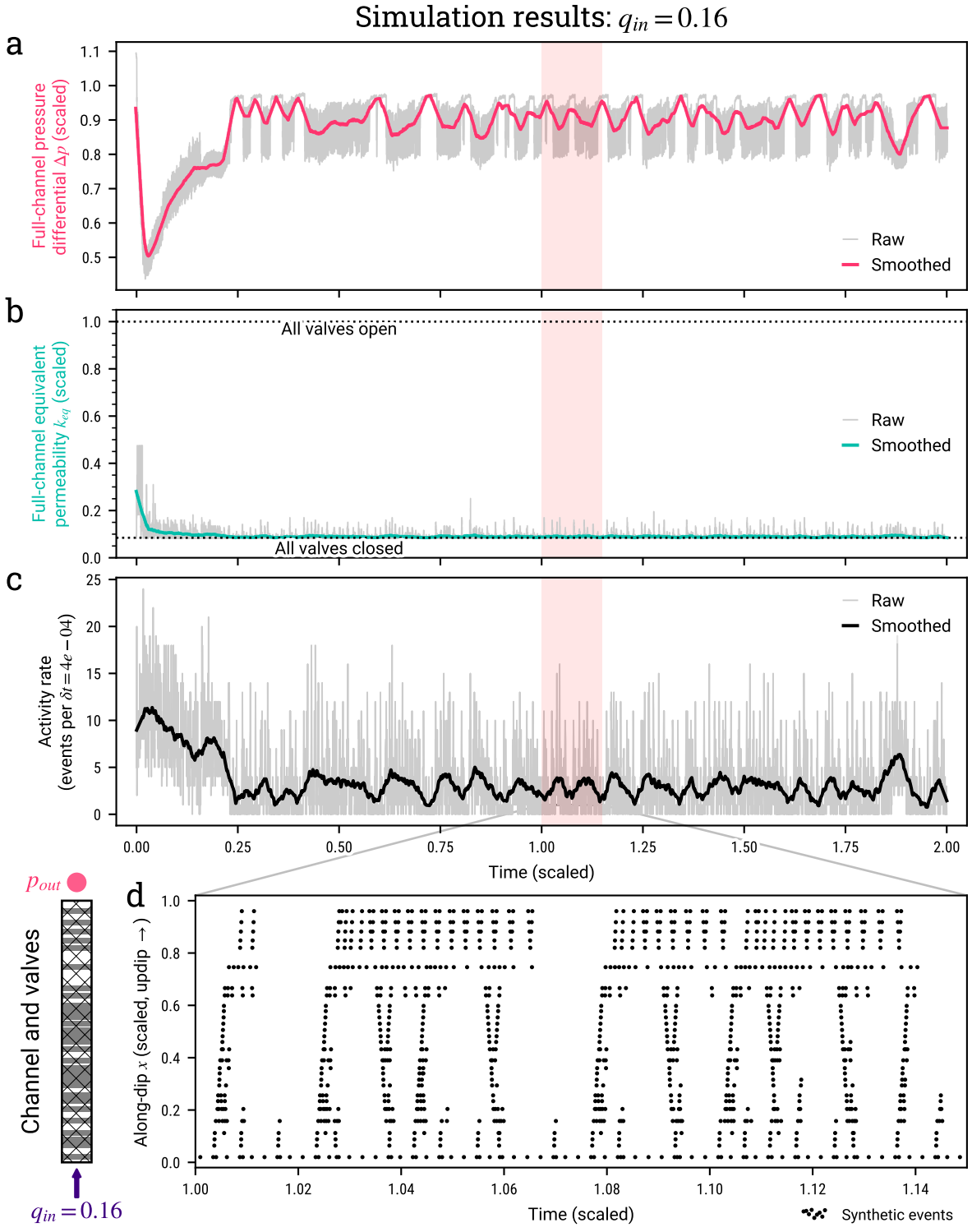

Figure 7: Time evolution of activity for a channel with 29 randomly distributed valves and a low input flux $q_{in} = 0.16$, just above q_c^{break}. *(a)* Fluid pressure differential across the channel Δp, *(b)* equivalent permeability k_{eq} and *(c)* activity rate (events per $\delta t = 4.10^{-4}$ scaled unit). Raw data in grey and smoothed time series in colors (rolling mean with a window of length $\tau = 0.03$). *d* Time-space diagram of events occurrence within the channel. All valves are initially closed. A permanent regime with intermittent activity is reached after a short initial transient.

This work was submitted to Journal of Geophysical Research: Solid Earth (19/02/2021)

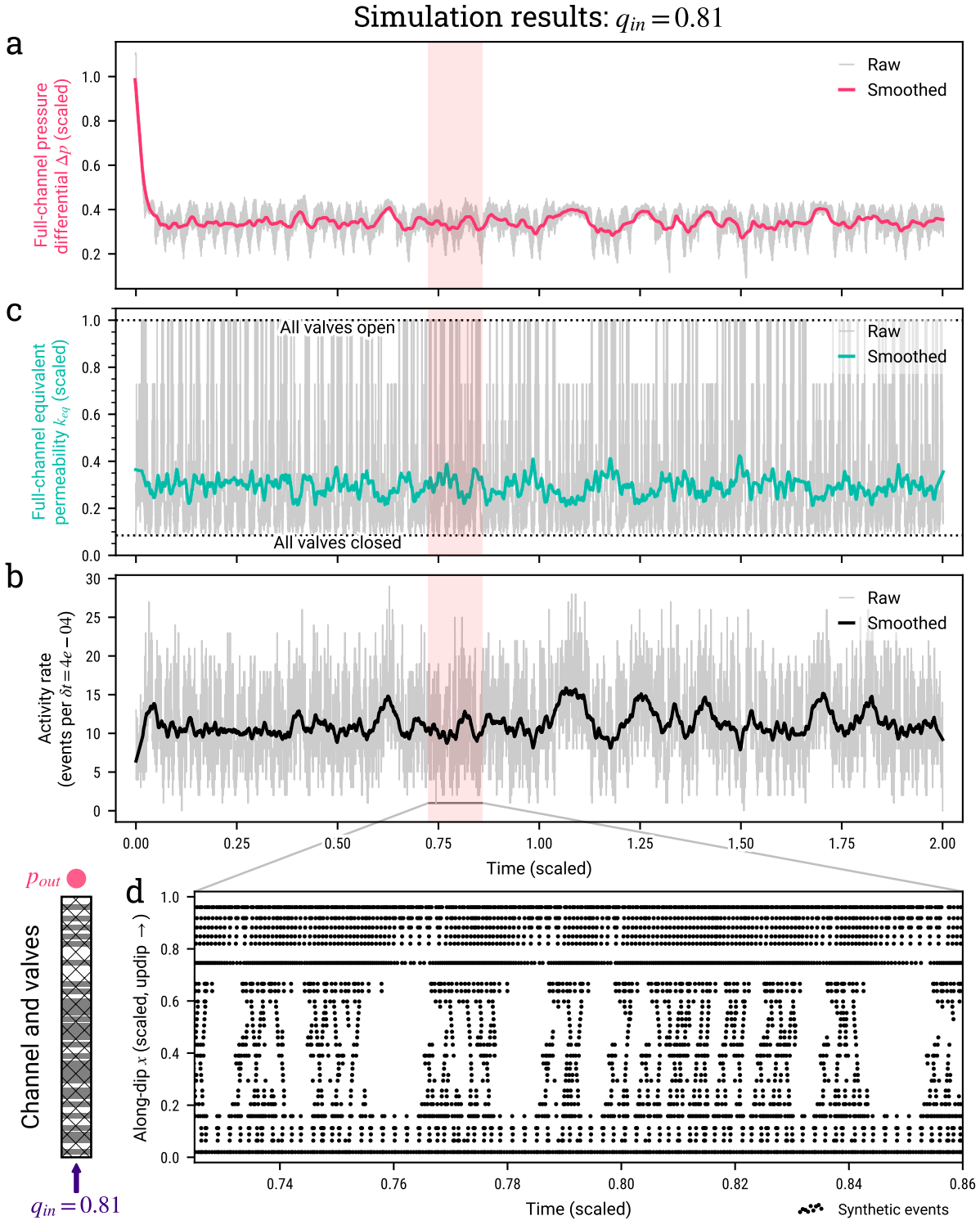

Figure 8: Time evolution of activity for a channel with 29 randomly distributed valves and a high input flux $q_{in} = 0.81$, just below q_c^{clog}. *(a)* Fluid pressure differential across the channel Δp, *(b)* equivalent permeability k_{eq} and *(c)* activity rate (events per $\delta t = 4.10^{-4}$ scaled unit). Raw data in grey and smoothed time series in colors (rolling mean with a window of length $\tau = 0.03$). *d* Time-space diagram of events occurrence within the channel. All valves are initially closed. A permanent regime with intermittent activity is reached after a short initial transient.

This work was submitted to Journal of Geophysical Research: Solid Earth (19/02/2021)

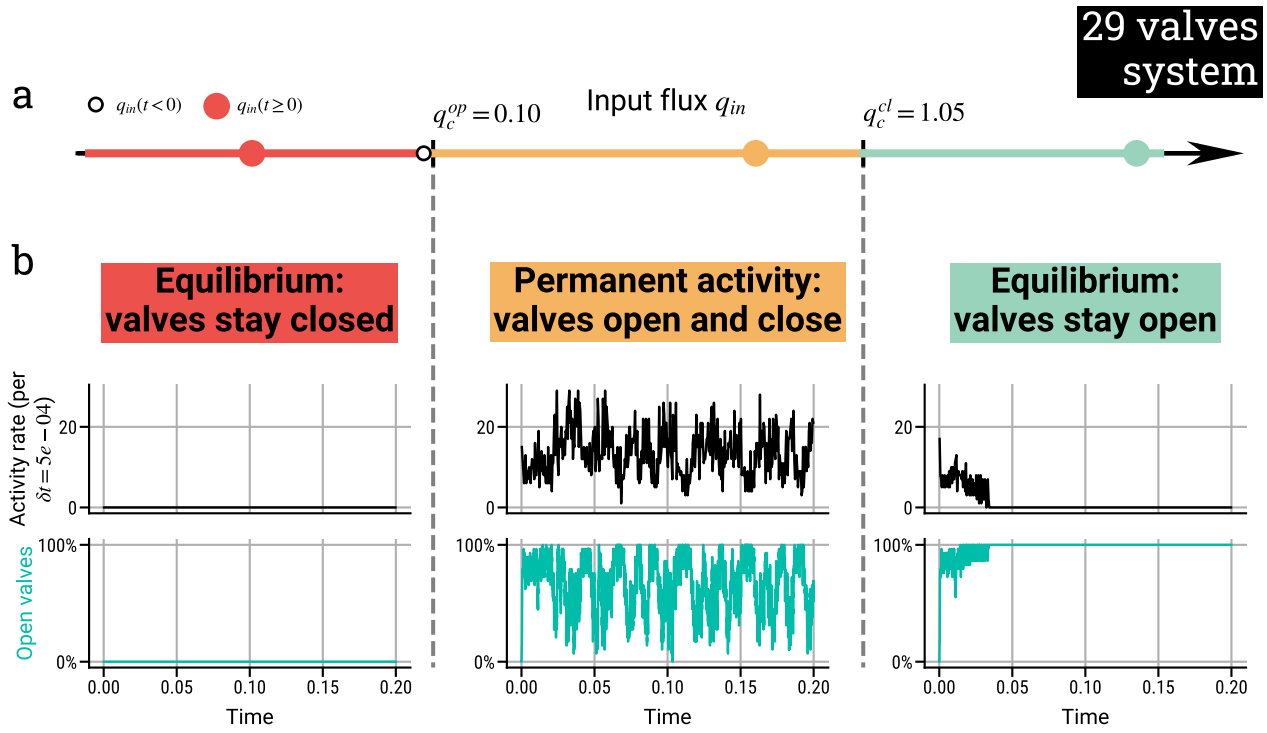

Figure 9: Influence of the input flux q_{in} in a system with 29, randomly distributed valves. *(a)* Three intervals of input flux q_{in} are delimited by two threshold values q_c^{clog} and q_c^{break}. *(b)* Examples of activity rate (number of events per $\delta t = 5.10^{-4}$, scaled unit, in black) and proportion of open valves (in cyan) as a function of time, starting at $t = 0$ with all valves closed.

where N_{cl} is the number of closed valves, and L is the channel length. For any of the three regimes, activity rate, k_{eq} and the pressure difference across the channel Δp reach a dynamic equilibrium around a stable value after an initial transient, thus defining a permanent regime (Figures 7 and 8).

As predicted by the analysis above, the value of the input flux determines the regime of activity that occurs during the permanent regime (Figure 9). Valve activity occurs when the flux is within the $q_c^{break} - q_c^{clog}$ range but, as shown in Figure 10, the style of activity varies significantly as a function of the input flux in the fault zone. Near the two ends of the $q_c^{clog} - q_c^{break}$ interval, activity in the permanent regime is episodic or time-clustered (see also Figures 7 and 8), and almost periodic for the highest values of q_{in} (Figures 11 and 12). For intermediate fluxes, activity in the permanent regime is random and Poisson-like, with a seemingly constant overall rate.

Here, the catalog of synthetic events in space and time is analyzed in the form of a two-dimensional point process (t_i, x_i) illustrated in time-location graphs (Figures 7d, 8d, 11 and 12c). To characterize the level of time clustering (episodicity) of synthetic events, we follow [36] and use statistical tools for the analysis of temporal point processes [61]. The main idea is to compute the spectrum of the signal count autocorrelations and to estimate its power-law exponent γ. A flat spectrum with $\gamma \approx 0$ corresponds to a nearly Poissonian process, whereas γ values that are significantly larger than 0 are indicative of time clustering.

In Figure 10a, we see that $\gamma \approx 0$ for intermediate values of the input flux. In this case, activity is Poisson-like. For near-threshold values of the input flux, activity is characterized by high values of γ, indicating time clustering. Time-series of the activity rate reveal episodic bursts (Figure 10b). When the input flux is low (close to q_c^{clog}), activity appears to be close to scale-invariant clustering with a burst recurrence rate that depends on the time scale of measurement. For higher values of the input flux close to the upper bound q_c^{break}, activity proceeds in quasi periodic bursts, whose period seem to increase with increasing q_{in}.

As the input flux is increased from the lower threshold value q_c^{break} to the upper one q_c^{clog}, the channel is increasingly open in average. Figure 10c shows average proportion of open valves in different simulations, as a function of q_{in}. Another way to look at this behaviour is to look at the proportion of open valves in time, which reflects the evolution of k_{eq}, the bulk permeability of the whole channel. For

This work was submitted to Journal of Geophysical Research: Solid Earth (19/02/2021)

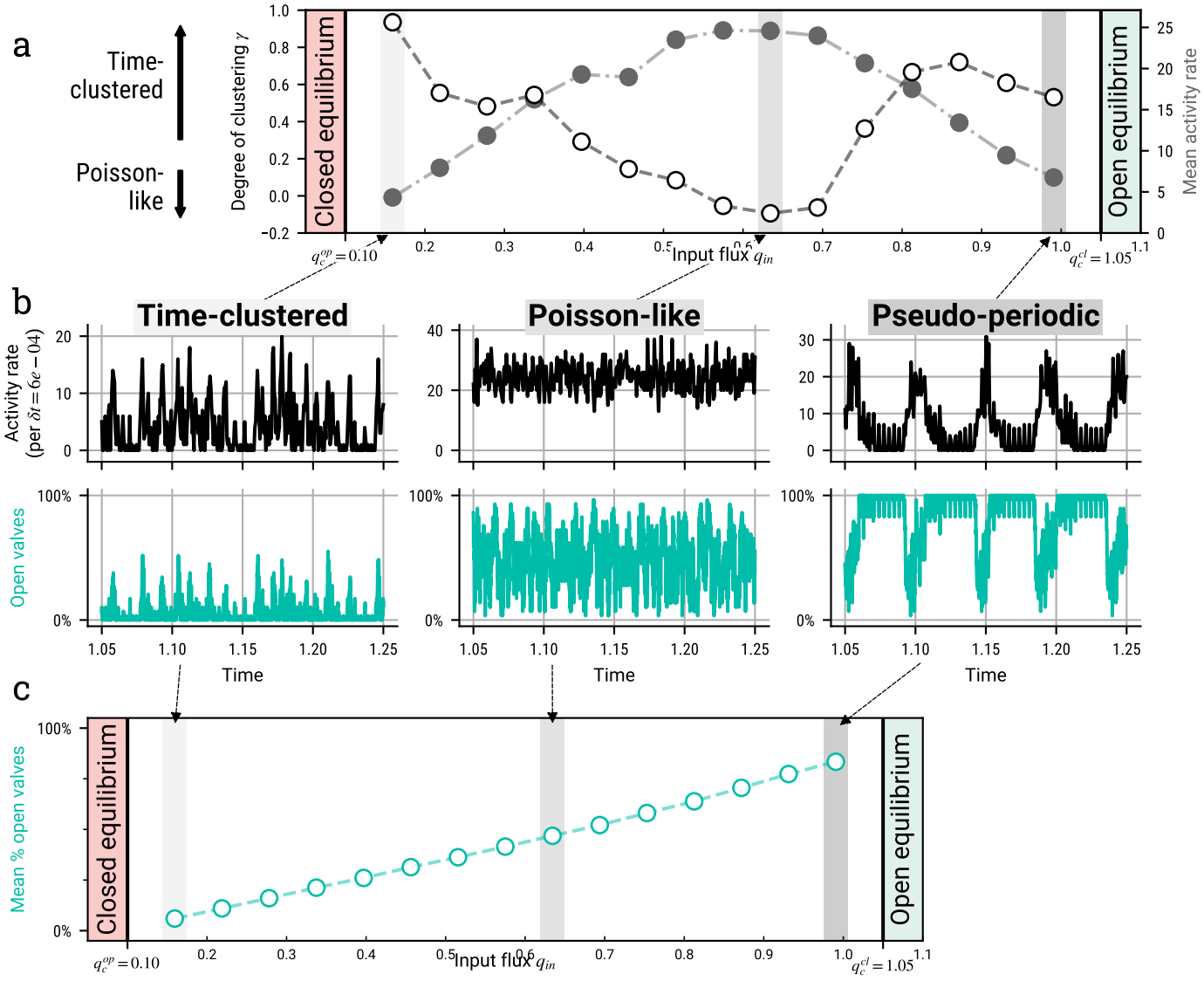

Figure 10: Different permanent activity styles as a function of the input fluid flux. *(a)* Level of time clustering γ (the spectral slope of autocorrelation of event counts, see text) and mean activity rate (number of events per unit time, in gray) as a function of input flux q_{in}. For γ close to 0, activity is Poisson-like with no time clustering. The higher γ is, the more clustered and episodic activity is. *(b)* Activity rate (in black) and proportion of open valves (in cyan) as a function of time for particular simulations within the different regimes. *(c)* Time-averaged proportion of open valves in simulations, as a function of input flux.

This work was submitted to Journal of Geophysical Research: Solid Earth (19/02/2021)

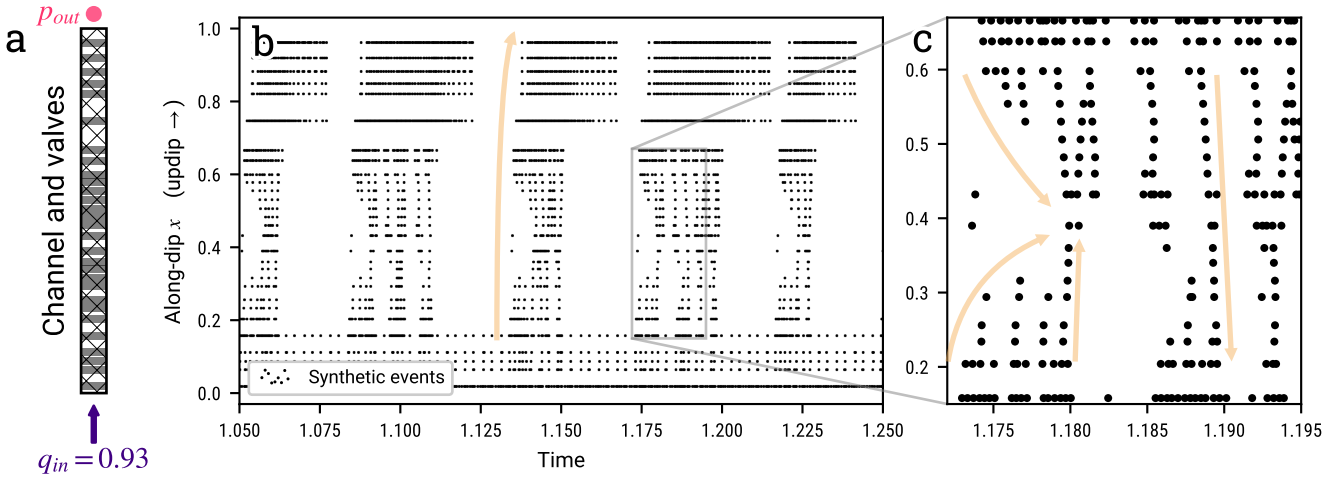

Figure 11: Synthetic tremor activity patterns. *(a)* Distribution of valves in the permeable channel. This distribution was generated randomly and contains three large clusters. *(b)* Activity patterns in space and time. Black dots stand for valve opening events. The lower valve cluster ($x = 0 - 0.18$) is active almost continuously. The middle and upper clusters ($x = 0.2 - 0.65$ and $x = 0.7 - 1$) is activated sequentially in bursts. Within a burst, activity is intermittent too. *(c)* focus on the activity in the middle valve cluster showing fast, short-scale migrations in both the updip and downdip directions.

a low input flux ($q_{in} \approx q_c^{break}$), valves are closed most of the time and bursts are linked to phases of valve openings. In the other extreme, for $q_{in} \approx q_c^{clog}$, permeability is open most of the time. Swarms of events then occur mainly when the channel shuts down temporarily and valve pressures increase until unclogging conditions are met.

5.1 Cascades and migrations of synthetic activity

In the random distribution of valves that was adopted here, there are three patches where valves are closer to one another than elsewhere, around $x = 0.1$, $x = 0.5$ and $x = 0.85$ (Figure 11). In patches of closely packed valves, the constructive interaction we describe in Figure 6 is responsible for the occurrence of rapid cascades of events. Those migrations propagate with an apparent speed that is faster than that for a constant diffusivity. Furthermore, these migrations may proceed in both downdip and updip directions. Obviously, the interaction is weaker and slower for valves that are separated by larger distances. Thus, the rates of cascading and event migration depend on the valve distribution.

Figure 11 depicts typical synthetic activity patterns. The input flux is close to the upper threshold q_c^{break}, $q_{in} = 0.93$. Figure 11c shows nearly deterministic patterns of collective behavior at both short time and space scales. Cascades of triggering/opening events are associated with migrations of activity that show up as oblique dot alignments in the time-location chart.

The fastest migrations appear to start and stop at the edges of densely populated patches. In such a patch, valves are close to one another and act in tandem. This shows up as an activity cluster which hosts its own internal migration patterns. Larger scale valve patches are activated sequentially in the updip direction. These large scale migrations proceed at slower rates than those within a single valve patch (Figure 11b).

5.2 Large-scale valving behavior

Segments of the channel containing a number of closely-spaced valves act like macroscopic valves, such that their equivalent permeability varies in hysteretical cycles with the total pressure difference across them. This behaviour is achieved over a large range of scales, from small sets of a few valves to large valve patches and eventually for the full channel. Figure 12 depicts the cycles of equivalent permeability k_{eq} and total pressure difference across the whole channel, noted Δp, for three cycles of channel activity. Pore-pressure accumulation and release varies in tandem with open/closed permeability switches, thus defining large-scale valving cycles coupled with the occurrence of seismic activity.

This work was submitted to Journal of Geophysical Research: Solid Earth (19/02/2021)

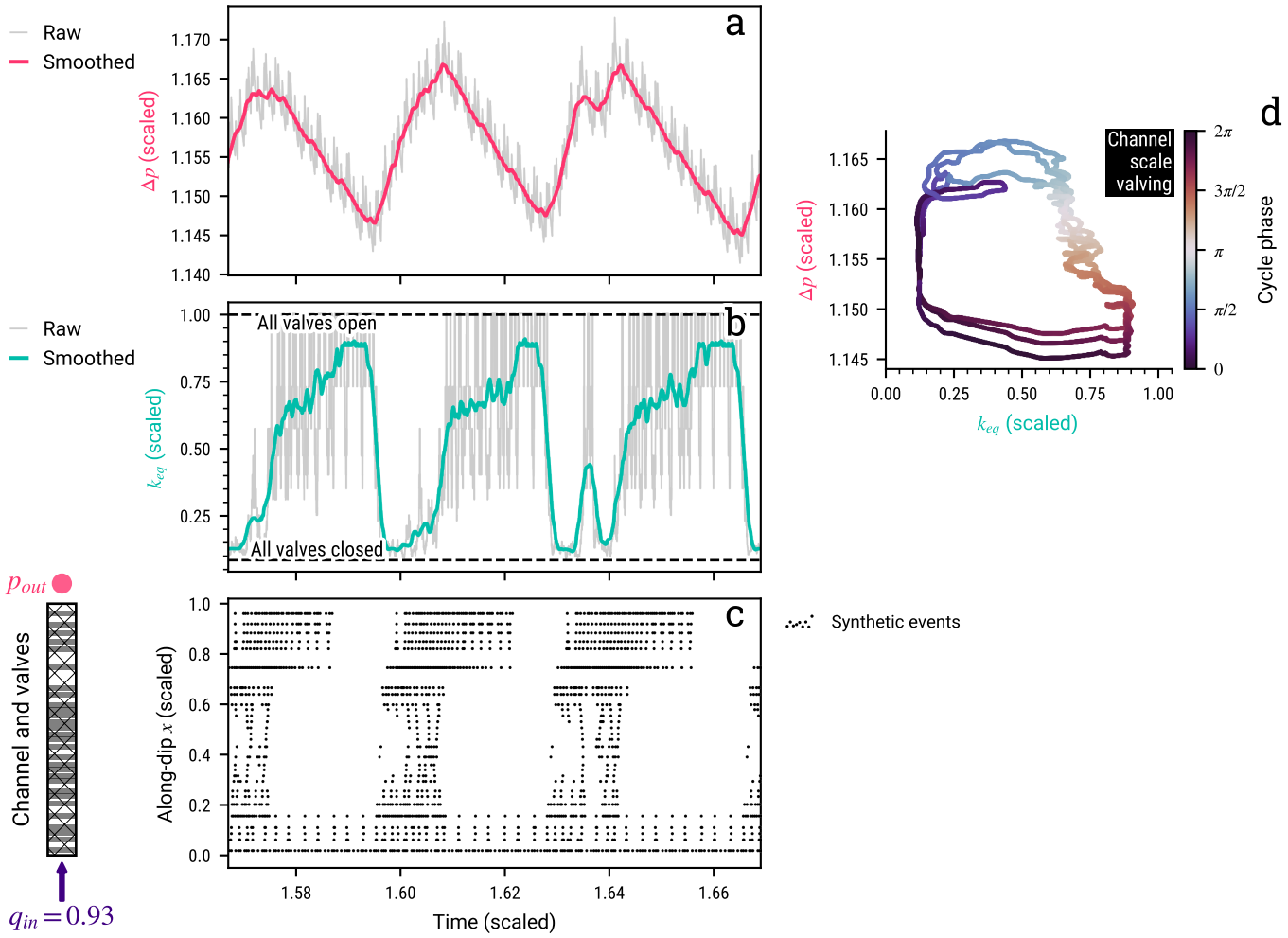

Figure 12: Cyclic variations of activity for $q_{in} = 0.93$. *(a)* Pore pressure difference across the whole channel Δp, *(b)* channel bulk permeability k_{eq}, and *(c)* time-location chart of events. *(d)* Activity in (Δp, k_{eq}) space, showing hysteretical cycles like those of a single valve.

This work was submitted to Journal of Geophysical Research: Solid Earth (19/02/2021)

6 Discussion

The key feature of the model is that pore-pressure diffusion induced by the opening of a valve is an efficient triggering mechanism for further valve openings. In spite of the model simplicity, the activity that is generated proceeds in complex migration and time clustering patterns that are comparable to seismic observations. An important result is that, for a given valve distribution, *i.e.* a given permeability structure of the channel, the style of activity that is produced depends on the input fluid flux.

6.1 Perspectives for diagnosing hydraulic conditions in real fault zones

According to this model, the rate and style of seismic activity depends on the hydraulic regime of the permeable channel. Thus, provided that the model is not fundamentally flawed, one can use LFE patterns to investigate the hydraulics of fault zones (and eventually other natural systems such as volcanoes or hydrothermal fields). Conversely, successful comparisons between simulated and observed activity patterns lend credence to the model. To this end, we now compare synthetic activity patterns with observations in Guerrero, Mexico (section 2.4, Figure 1).

We first observe that activity migrates in both the updip and downdip directions within the sweet spot patch at rates that are faster than that from the sweet spot to the transient zone (Figure 1), as in our simulations. On the longest timescale, LFE activity in Guerrero appears time-clustered [33, 36]. Activity bursts recur in episodic fashion and are mostly concentrated in the downdip sweet spot patch. At times, during the most vigorous episodes, activity crosses over into the less active updip transient zone. Our model generates a similar pattern when the input flux q_{in} is near threshold values. At the lower end of the dimensionless operating flux range (*i.e.* $q_c^{break} - q_c^{clog}$), the channel is mostly closed and activity emerges when it opens up in episodic fashion. In contrast, at the upper end of the flux range, the channel is mostly open and activity bursts are concentrated at the times of partial channel closure. Therefore, two different sets of values for valve opening/closing δp thresholds, valve permeability and q_{in} could correspond to the Guerrero activity. The first situation is reminiscent of a fault-valve mechanism, as high fault zone permeability correlates in time with seismicity. Several studies interpret tremor activity in Guerrero using this correlation [26, 35]. In the framework of our model, however, the second situation seems as likely as the first one. We thus argue that seismicity bursts may not be systematically linked to an increase of fault permeability and subsequent fluid pressure surge, but may also be due to episodic phases of clogging in the fault, leading to transient fluid pressure build-up and release.

In our calculations, the lowermost patch is always active and is at the origin of larger scale migrations towards the less active upper patch, which trigger activity there. This is reminiscent of what happens in Guerrero (Figure 1). This behaviour is a consequence of the boundary conditions that are imposed in the model. At the base of the channel, the fixed input flux constantly stimulates activity whereas the fixed pressure that is imposed at the top acts to buffer pressure variations. Thus, activation of the upper valve cluster only occurs once large pore pressures and fluid volumes have built up in the lower part of the channel.

6.2 Possible extensions of the model

The present hydraulic model was designed to evaluate the potential of the clogging/unclogging valve mechanism and to illustrate the various types of activity that can be generated. It can be made more complex in many ways. As discussed above, the migration and spatial patterns of activity depend on the distribution of valves and other valve distributions should be investigated. The density of valves can be related to the roughness of the subduction interface, which may be inherited from seafloor sedimentary cover or topography prior to subduction. We do not expect, however, to discover new activity regimes because solutions are determined by the four valve control parameters introduced above. Other boundary conditions than those used here are worth investigating. In particular, dehydration surges may occur due for example to kinetic constraints on metamorphic reactions or to highly hydrated portions of the downgoing plate crossing the phase-change boundary. Ultimately, one should investigate randomized valve characteristics and allow for time-dependent opening and closure processes.

An important direction to explore in the future is the coupling between hydraulic transients and fault slip. The latter can be described using a RSF friction parameterization with coefficients that depend on pore pressure [62]. In such a model, key issues are the causal relationships between pore pressure transients, in-channel damage (valve opening), and slip. As discussed in the introduction, most models of faulting consider that slip comes first and induces a permeability increase through fracturing and dilation. A key factor is a high pore pressure because it lowers the fault strength. At the same time,

This work was submitted to Journal of Geophysical Research: Solid Earth (19/02/2021)

however, the average strength of the fault may well be controlled by closed valves that mechanically act as slip barriers. On the one hand, unclogging lowers the friction coefficient because it reduces the solid-to-solid contact area. On the other hand, it also acts to limit the magnitude of the pore pressure rise. Thus, one can have plugs that resist unclogging and fail due to very high pore pressures, and others that get unclogged and fail due to a reduced friction coefficient.

7 Conclusion

We have shown that clogging and unclogging events in a permeable plug follow one another logically in a simple valve mechanism. We have further shown that quantitative requirements for the mechanism to work are met in geological conditions. In an analysis of valve-to-valve interaction, we have found that the behaviour of a permeable channel containing valves depends on two valve parameters (pressure ratio $\delta p_c^{break}/\delta p_c^{clog}$ and permeability ratio k_{hi}/k_{lo}). In one case, the channel is in a stable steady-state regime for all values of the input flux. In the other case, the channel is unstable with valves that open up and close down repeatedly if the input flux is within a certain range. We have shown that only the latter is relevant to geological systems and that the activity patterns that are generated are very similar to those that are observed in many subduction zones.

Using this model and more elaborate versions of it, one may hope to use microseismicity patterns to probe into the hydraulics of permeable fault zones and how they change with time. For given valve parameters that meet the condition for instability ($\delta p_c^{break}/\delta p_c^{clog} < k_{hi}/k_{lo}$), the activity regime depends on a dimensionless input rate of fluid into the channel. This dimensionless input rate is calculated with respect to a Darcy flux for some reference permeability value (chosen to be k_{hi} here). For application to natural conditions, the same dimensionless input rate can be obtained for different pairs of fluid flux and permeability values. Conversely, the same fluid flux may be responsible for different activity styles in different parts of the subduction interface depending on the local permeability value. In addition, time changes of the fluid flux, due for example to the subduction of more or less hydrated parts of an oceanic plate, may induce changes of activity.

The rate of fluid release by metamorphic reactions depends on the subduction rate and on the type of material that dehydrates. One can hardly expect that it is the same everywhere as, for example, subduction rates vary by almost one order of magnitude. Therefore, comparing seismicity patterns in different subduction zones is likely to prove very useful. In particular, one should pay attention to subduction zone segments that do not seem to generate LFE activity [*e.g., 18]*. As shown in this paper, this may be due to a fluid flux that is either very high or very small.

Acknowledgments

This study was supported by the European Research Council under the European Union Horizon 2020 research and innovation program (Grant Agreement 787399-SEISMAZE). Numerical computations were performed on the S-CAPAD platform, IPGP, France. All figures were produced using Matplotlib [45]. The LFE catalog in Guerrero, Mexico is made available on the Slow-Earthquake database, under the name Frank2014 (http://www-solid.eps.s.u-tokyo.ac.jp/ sloweq/).

References

[1] Gbedo Constant Agbangla, Patrice Bacchin, and Eric Climent. Collective dynamics of flowing colloids during pore clogging. *Soft Matter*, 10(33):6303–6315, 2014. doi:10.1039/C4SM00869C.

[2] Takashi Amagai, Atsushi Okamoto, Takamasa Niibe, Nobuo Hirano, Kenichi Motomiya, and Noriyoshi Tsuchiya. Silica nanoparticles produced by explosive flash vaporization during earthquakes. *Scientific Reports*, 9(1):9738, December 2019. ISSN 2045-2322. doi:10.1038/s41598-019-46320-7.

[3] Samuel Angiboust, Thomas Pettke, Jan C. M. De Hoog, Benoit Caron, and Onno Oncken. Channelized Fluid Flow and Eclogite-facies Metasomatism along the Subduction Shear Zone. *Journal of Petrology*, 55(5):883–916, May 2014. ISSN 1460-2415, 0022-3530. doi:10.1093/petrology/egu010.

[4] Samuel Angiboust, Josephine Kirsch, Onno Oncken, Johannes Glodny, Patrick Monié, and Erik Rybacki. Probing the transition between seismically coupled and decoupled segments along an ancient subduction interface. *Geochemistry, Geophysics, Geosystems*, 16(6):1905–1922, June 2015. ISSN 15252027. doi:10.1002/2015GC005776.

[5] Hideo Aochi, Blanche Poisson, Renaud Toussaint, Xavier Rachez, and Jean Schmittbuhl. Self-induced seismicity due to fluid circulation along faults. *Geophysical Journal International*, 196(3):1544–1563, December 2013. ISSN 0956-540X. doi:10.1093/gji/ggt356. https://academic.oup.com/gji/article-pdf/196/3/1544/1554288/ggt356.pdf.

[6] Pascal Audet and YoungHee Kim. Teleseismic constraints on the geological environment of deep episodic slow earthquakes in subduction zone forearcs: A review. *Tectonophysics*, 670:1–15, February 2016. ISSN 00401951. doi:10.1016/j.tecto.2016.01.005.

[7] H. Auradou, G. Drazer, J. P. Hulin, and J. Koplik. Permeability anisotropy induced by the shear displacement of rough fracture walls. *Water Resources Research*, 41(9):09423, September 2005. doi:10.1029/2005WR003938.

[8] Sylvain Barbot. Slow-slip, slow earthquakes, period-two cycles, full and partial ruptures, and deterministic chaos in a single asperity fault. *Tectonophysics*, 768:228171, 2019. ISSN 0040-1951. doi:10.1016/j.tecto.2019.228171.

[9] Eric Beaucé, William B. Frank, Anne Paul, Michel Campillo, and Robert D. Hilst. Systematic Detection of Clustered Seismicity Beneath the Southwestern Alps. *Journal of Geophysical Research: Solid Earth*, 124(11):11531–11548, November 2019. ISSN 2169-9313, 2169-9356. doi:10.1029/2019JB018110.

[10] Lauren E. Beckingham. Evaluation of macroscopic porosity-permeability relationships in heterogeneous mineral dissolution and precipitation scenarios. *Water Resources Research*, 53(12):10217–10230, 2017. doi:10.1002/2017WR021306. https://agupubs.onlinelibrary.wiley.com/doi/pdf/10.1002/2017WR021306.

[11] N. M. Beeler, Amanda Thomas, Roland Bürgmann, and David Shelly. Inferring fault rheology from low-frequency earthquakes on the San Andreas. *Journal of Geophysical Research: Solid Earth*, 118 (11):5976–5990, November 2013. ISSN 21699313. doi:10.1002/2013JB010118.

[12] Whitney M. Behr and Roland Bürgmann. What's down there? The structures, materials and environment of deep-seated slow slip and tremor. *Philosophical Transactions of the Royal Society A: Mathematical, Physical and Engineering Sciences*, 379(2193):20200218, March 2021. ISSN 1364-503X, 1471-2962. doi:10.1098/rsta.2020.0218.

[13] Yehuda Ben-Zion. Episodic tremor and slip on a frictional interface with critical zero weakening in elastic solid. *Geophysical Journal International*, 189(2): 1159–1168, May 2012. ISSN 0956-540X. doi:10.1111/j.1365-246X.2012.05422.x. https://academic.oup.com/gji/article-pdf/189/2/1159/17364854/189-2-1159.pdf.

[14] Philip M Benson, Sergio Vinciguerra, Philip G Meredith, and R Paul Young. Laboratory simulation of volcano seismicity. *Science*, 322(5899):249–252, 2008. ISSN 0036-8075. doi:10.1126/science.1161927. https://science.sciencemag.org/content/322/5899/249.full.pdf.

[15] Gregory C. Beroza and Satoshi Ide. Slow Earthquakes and Nonvolcanic Tremor. *Annual Review of Earth and Planetary Sciences*, 39(1):271–296, May 2011. ISSN 0084-6597, 1545-4495. doi:10.1146/annurev-earth-040809-152531.

[16] Filippo Bianchi, Marcel Thielmann, Lucilla de Arcangelis, and Hans Jürgen Herrmann. Critical Bursts in Filtration. *Physical Review Letters*, 120(3):034503, January 2018. ISSN 0031-9007, 1079-7114. doi:10.1103/PhysRevLett.120.034503.

[17] Filippo Bianchi, Falk K. Wittel, Marcel Thielmann, Pavel Trtik, and Hans J. Herrmann. Tomographic Study of Internal Erosion of Particle Flows in Porous Media. *Transport in Porous Media*, 122(1):169–184, March 2018. ISSN 0169-3913, 1573-1634. doi:10.1007/s11242-017-0996-8. arXiv:1709.00221.

[18] G. M. Bocchini, P. Martínez-Garzón, R. M. Harrington, and M. Bohnhoff. Does Deep Tectonic Tremor Occur in the Central-Eastern Mediterranean Basin? *Journal of Geophysical Research: Solid Earth*, 126(1):2020JB020448, 2021. ISSN 2169-9356. doi:10.1029/2020JB020448.

[19] M. G. Bostock, A. A. Royer, E. H. Hearn, and S. M. Peacock. Low frequency earthquakes below southern Vancouver Island. *Geochemistry, Geophysics, Geosystems*, 13(11):n/a–n/a, November 2012. ISSN 15252027. doi:10.1029/2012GC004391.

[20] M. G. Bostock, A. M. Thomas, G. Savard, L. Chuang, and A. M. Rubin. Magnitudes and moment-duration scaling of low-frequency earthquakes beneath southern Vancouver Island. *Journal of Geophysical Research: Solid Earth*, 120(9):6329–6350, 2015. ISSN 2169-9356. doi:10.1002/2015JB012195.

[21] Michael R. Brudzinski and Richard M. Allen. Segmentation in episodic tremor and slip all along Cascadia. *Geology*, 35(10):907–910, October 2007. ISSN 0091-7613. doi:10.1130/G23740A.1. https://pubs.geoscienceworld.org/geology/article-pdf/35/10/907/3533023/i0091-7613-35-10-907.pdf

[22] Thibault Candela, Emily E. Brodsky, Chris Marone, and Derek Elsworth. Laboratory evidence for particle mobilization as a mechanism for permeability enhancement via dynamic stressing. *Earth and Planetary Science Letters*, 392:279–291, April 2014. ISSN 0012821X. doi:10.1016/j.epsl.2014.02.025.

[23] S. R. Chestler and K. C. Creager. Evidence for a scale-limited low-frequency earthquake source process. *Journal of Geophysical Research: Solid Earth*, 122(4):3099–3114, 2017. ISSN 2169-9356. doi:10.1002/2016JB013717.

[24] Bernard A. Chouet. Long-period volcano seismicity: Its source and use in eruption forecasting. *Nature*, 380(6572):309, March 1996. ISSN 1476-4687. doi:10.1038/380309a0.

[25] Faruk Civan. Modified formulations of particle deposition and removal kinetics in saturated porous media. *Transp Porous Med*, 111:381–410, 2016. doi:10.1007/s11242-015-0600-z.

[26] Víctor M. Cruz-Atienza, Carlos Villafuerte, and Harsha S. Bhat. Rapid tremor migration and pore-pressure waves in subduction zones. *Nature Communications*, 9(1), December 2018. ISSN 2041-1723. doi:10.1038/s41467-018-05150-3.

[27] Brent G. Delbridge, Joshua D. Carmichael, Robert M. Nadeau, David R. Shelly, and Roland Bürgmann. Geodetic Measurements of Slow-Slip Events Southeast of Parkfield, CA. *Journal of Geophysical Research: Solid Earth*, 125(5), May 2020. ISSN 2169-9313, 2169-9356. doi:10.1029/2019JB019059.

[28] N. Delouche, A. B. Schofield, and H. Tabuteau. Dynamics of progressive pore clogging by colloidal aggregates. *Soft Matter*, 16(43):9899–9907, 2020. doi:10.1039/D0SM01403F.

[29] James H. Dieterich. Earthquake nucleation on faults with rate-and state-dependent strength. *Tectonophysics*, 211(1):115–134, 1992. ISSN 0040-1951. doi:10.1016/0040-1951(92)90055-B.

[30] Åke Fagereng and Richard H. Sibson. Mélange rheology and seismic style. *Geology*, 38(8):751–754, August 2010. ISSN 1943-2682, 0091-7613. doi:10.1130/G30868.1.

[31] Gaspard Farge, Nikolaï M. Shapiro, and William B. Frank. Moment-Duration Scaling of Low-Frequency Earthquakes in Guerrero, Mexico. *Journal of Geophysical Research: Solid Earth*, 125 (8), August 2020. ISSN 2169-9313, 2169-9356. doi:10.1029/2019JB019099.

[32] William B. Frank, Nikolaï M. Shapiro, Vladimir Kostoglodov, Allen L. Husker, Michel Campillo, Juan S. Payero, and Germán A. Prieto. Low-frequency earthquakes in the Mexican Sweet Spot: LFES IN THE MEXICAN SWEET SPOT. *Geophysical Research Letters*, 40(11):2661–2666, June 2013. ISSN 00948276. doi:10.1002/grl.50561.

[33] William B. Frank, Nikolaï M. Shapiro, Allen L. Husker, Vladimir Kostoglodov, Alexey Romanenko, and Michel Campillo. Using systematically characterized low-frequency earthquakes as a fault probe in Guerrero, Mexico. *Journal of Geophysical Research: Solid Earth*, 119(10):7686–7700, October 2014. ISSN 21699313. doi:10.1002/2014JB011457.

[34] William B. Frank, Mathilde Radiguet, Baptiste Rousset, Nikolaï M. Shapiro, Allen L. Husker, Vladimir Kostoglodov, Nathalie Cotte, and Michel Campillo. Uncovering the geodetic signature of silent slip through repeating earthquakes: UNCOVERING SILENT SLIP. *Geophysical Research Letters*, 42(8):2774–2779, April 2015. ISSN 00948276. doi:10.1002/2015GL063685.

[35] William B. Frank, Nikolai M. Shapiro, Allen L. Husker, Vladimir Kostoglodov, Harsha S. Bhat, and M. Campillo. Along-fault pore-pressure evolution during a slow-slip event in Guerrero, Mexico. *Earth and Planetary Science Letters*, 413:135–143, March 2015. ISSN 0012821X. doi:10.1016/j.epsl.2014.12.051.

[36] William B. Frank, Nikolaï M. Shapiro, Allen L. Husker, Vladimir Kostoglodov, Alexander A. Gusev, and Michel Campillo. The evolving interaction of low-frequency earthquakes during transient slip. *Science Advances*, 2(4):e1501616, April 2016. ISSN 2375-2548. doi:10.1126/sciadv.1501616.

[37] Maria L. Frezzotti and Simona Ferrando. The chemical behavior of fluids released during deep subduction based on fluid inclusions. *American Mineralogist*, 100:352–377, 2015. doi:10.2138/am-2015-4933.

[38] Behzad Ghanbarian, Allen G. Hunt, Robert P. Ewing, and Muhammad Sahimi. Tortuosity in porous media: A critical review. *Soil Science Society of America Journal*, 77(5):1461–1477, 2013. doi:10.2136/sssaj2012.0435. https://acsess.onlinelibrary.wiley.com/doi/pdf/10.2136/sssaj2012.0435.

[39] Abhijit Ghosh, John E. Vidale, Justin R. Sweet, Kenneth C. Creager, Aaron G. Wech, Heidi Houston, and Emily E. Brodsky. Rapid, continuous streaking of tremor in Cascadia. *Geochemistry, Geophysics, Geosystems*, 11(12):n/a–n/a, December 2010. ISSN 15252027. doi:10.1029/2010GC003305.

[40] Silvio B. Giger, Eric Tenthorey, Stephen F. Cox, and John D. Fitz Gerald. Permeability evolution in quartz fault gouges under hydrothermal conditions. *Journal of Geophysical Research*, 112(B7), July 2007. ISSN 0148-0227. doi:10.1029/2006JB004828.

[41] J. Gomberg, A. Wech, K. Creager, K. Obara, and D. Agnew. Reconsidering earthquake scaling. *Geophysical Research Letters*, 43(12):6243–6251, June 2016. ISSN 00948276. doi:10.1002/2016GL069967.

[42] Jeremy M. Gosselin, Pascal Audet, Clément Estève, Morgan McLellan, Stephen G. Mosher, and Andrew J. Schaeffer. Seismic evidence for megathrust fault-valve behavior during episodic tremor and slip. *Science Advances*, 6(4):eaay5174, January 2020. ISSN 2375-2548. doi:10.1126/sciadv.aay5174.

[43] Gavin Hayes. Slab2 - A Comprehensive Subduction Zone Geometry Model, 2018.

[44] Heidi Houston, Brent G. Delbridge, Aaron G. Wech, and Kenneth C. Creager. Rapid tremor reversals in Cascadia generated by a weakened plate interface. *Nature Geoscience*, 4(6):404–409, June 2011. ISSN 1752-0908. doi:10.1038/ngeo1157.

[45] J. D. Hunter. Matplotlib: A 2D graphics environment. *Computing in Science & Engineering*, 9 (3):90–95, 2007. doi:10.1109/MCSE.2007.55.

[46] Husker, Allen L., Vladimir Kostoglodov, Victor M. Cruz-Atienza, Denis Legrand, Nikolai M. Shapiro, Juan S. Payero, Michel Campillo, and Eduardo Huesca-Pérez. Temporal variations of non-volcanic tremor (NVT) locations in the Mexican subduction zone: Finding the NVT sweet spot. *Geochemistry, Geophysics, Geosystems*, 13(3):Q03011, 2012. ISSN 1525-2027. doi:10.1029/2011GC003916.

[47] R. D. Hyndman, P. A. McCrory, A. Wech, H. Kao, and J. Ague. Cascadia subducting plate fluids channelled to fore-arc mantle corner: ETS and silica deposition. *Journal of Geophysical Research: Solid Earth*, 120(6):4344–4358, June 2015. ISSN 21699313. doi:10.1002/2015JB011920.

[48] Satoshi Ide. Striations, duration, migration and tidal response in deep tremor. *Nature*, 466(7304): 356–359, July 2010. ISSN 0028-0836, 1476-4687. doi:10.1038/nature09251.

[49] Satoshi Ide. Variety and spatial heterogeneity of tectonic tremor worldwide. *Journal of Geophysical Research: Solid Earth*, 117(B3), March 2012. ISSN 01480227. doi:10.1029/2011JB008840.

[50] Satoshi Ide. Modeling fast and slow earthquakes at various scales. *Proceedings of the Japan Academy. Series B, Physical and biological sciences*, 90(8):259–277, 2014. doi:10.2183/pjab.90.259.

[51] Koki Idehara, Suguru Yabe, and Satoshi Ide. Regional and global variations in the temporal clustering of tectonic tremor activity. *Earth, Planets and Space*, 66(1):66, December 2014. ISSN 1880-5981. doi:10.1186/1880-5981-66-66.

[52] Kyungjae Im, Derek Elsworth, and Chaoyi Wang. Cyclic permeability evolution during repose then reactivation of fractures and faults. *Journal of Geophysical Research: Solid Earth*, 124(5):4492–4506, 2019. doi:10.1029/2019JB017309. https://agupubs.onlinelibrary.wiley.com/doi/pdf/10.1029/2019JB017309.

[53] R. Jäger, M. Mendoza, and H. J. Herrmann. Channelization in porous media driven by erosion and deposition. *Physical Review E*, 95(1):013110, January 2017. ISSN 2470-0045, 2470-0053. doi:10.1103/PhysRevE.95.013110.

[54] Robin Jäger, Miller Mendoza, and Hans J. Herrmann. The Mechanism behind Erosive Bursts in Porous Media. *Physical Review Letters*, 119(12):124501, September 2017. ISSN 0031-9007, 1079-7114. doi:10.1103/PhysRevLett.119.124501. arXiv:1709.08451.

[55] Honn Kao, Shao-Ju Shan, Herb Dragert, Garry Rogers, John F. Cassidy, and Kumar Ramachandran. A wide depth distribution of seismic tremors along the northern Cascadia margin. *Nature*, 436:841–844, 2005. doi:10.1038/nature03903.

[56] Honn Kao, Shao-Ju Shan, Herb Dragert, and Garry Rogers. Northern Cascadia episodic tremor and slip: A decade of tremor observations from 1997 to 2007: NORTHERN CASCADIA ETS. *Journal of Geophysical Research: Solid Earth*, 114(B11), November 2009. ISSN 01480227. doi:10.1029/2008JB006046.

[57] Vladimir Kostoglodov, Allen Husker, Nikolai M. Shapiro, Juan S. Payero, Michel Campillo, Nathalie Cotte, and Robert Clayton. The 2006 slow slip event and nonvolcanic tremor in the Mexican subduction zone. *Geophysical Research Letters*, 37(24):L24301, 2010. ISSN 1944-8007. doi:10.1029/2010GL045424.

[58] Alissa J. Kotowski and Whitney M. Behr. Length scales and types of heterogeneities along the deep subduction interface: Insights from exhumed rocks on Syros Island, Greece. *Geosphere*, 15 (4):1038–1065, August 2019. ISSN 1553-040X. doi:10.1130/GES02037.1.

[59] Arshad Kudrolli and Xavier Clotet. Evolution of Porosity and Channelization of an Erosive Medium Driven by Fluid Flow. *Physical Review Letters*, 117(2):028001, July 2016. ISSN 0031-9007, 1079-7114. doi:10.1103/PhysRevLett.117.028001.

[60] Yajing Liu and James R. Rice. Spontaneous and triggered aseismic deformation transients in a subduction fault model. *Journal of Geophysical Research: Solid Earth*, 112(B9), 2007. doi:10.1029/2007JB004930. https://agupubs.onlinelibrary.wiley.com/doi/pdf/10.1029/2007JB004930.

[61] S. B. Lowen and M. C. Teich. *Fractal-Based Point Processes*, volume 366 of *Wiley Series in Probability and Statistics*. John Wiley and Sons, Inc, Hoboken, New Jersey, 2005.

[62] Yingdi Luo and Zhen Liu. Rate-and-State Model Casts New Insight into Episodic Tremor and Slow-slip Variability in Cascadia. *Geophysical Research Letters*, page 11, 2019.

[63] Michael Manga, Igor Beresnev, Emily E. Brodsky, Jean E. Elkhoury, Derek Elsworth, S. E. Ingebritsen, David C. Mays, and Chi-Yuen Wang. Changes in permeability caused by transient stresses: Field observations, experiments, and mechanisms. *Reviews of Geophysics*, 50(2), 2012. doi:10.1029/2011RG000382. https://agupubs.onlinelibrary.wiley.com/doi/pdf/10.1029/2011RG000382.

[64] Craig E Manning. Coupled reaction and flow in subduction zones: Silica metasomatism in the mantle wedge. In *Fluid Flow and Transport in Rocks*, pages 139–148. Springer, 1997.

[65] Laura M. McDowell-Boyer, James R. Hunt, and Nicholas Sitar. Particle transport through porous media. *Water Resources Research*, 22(13):1901–1921, 1986. doi:10.1029/WR022i013p01901. https://agupubs.onlinelibrary.wiley.com/doi/pdf/10.1029/WR022i013p01901.

[66] Oleg Melnik, Vladimir Lyakhovsky, Nikolai M. Shapiro, Natalia Galina, and Olga Bergal-Kuvikas. Deep long period volcanic earthquakes generated by degassing of volatile-rich basaltic magmas. *Nature Communications*, 11(1):3918, 2020. doi:10.1038/s41467-020-17759-4.

[67] Stephen A Miller and Amos Nur. Permeability as a toggle switch in fluid-controlled crustal processes. *Earth and Planetary Science Letters*, page 14, 2000.

[68] M. Moura, K. J. Måløy, and R. Toussaint. Critical behavior in porous media flow. *EPL (Europhysics Letters)*, 118(1):14004, April 2017. ISSN 0295-5075, 1286-4854. doi:10.1209/0295-5075/118/14004.

[69] Kazushige Obara. Nonvolcanic deep tremor associated with subduction in southwest japan. *Science*, 296(5573):1679–1681, 2002. ISSN 0036-8075. doi:10.1126/science.1070378. http://science.sciencemag.org/content/296/5573/1679.full.pdf.

[70] Atsushi Okamoto. Formation of silica particles from supercritical fluids and its impacts on the hydrological properties in the crust. In *EGU General Assembly Conference Abstracts*, volume 21, page 4614, Vienna, April 2019.

[71] Juan S. Payero, Vladimir Kostoglodov, Nikolai Shapiro, Takeshi Mikumo, Arturo Iglesias, Xyoli Pérez-Campos, and Robert W. Clayton. Nonvolcanic tremor observed in the Mexican subduction zone. *Geophysical Research Letters*, 35(7):L07305, 2008. ISSN 1944-8007. doi:10.1029/2007GL032877.

[72] S. M. Peacock, N. I. Christensen, M. G. Bostock, and P. Audet. High pore pressures and porosity at 35 km depth in the Cascadia subduction zone. *Geology*, 39(5):471–474, May 2011. ISSN 0091-7613, 1943-2682. doi:10.1130/G31649.1.

[73] John P. Platt, Haoran Xia, and William Lamborn Schmidt. Rheology and stress in subduction zones around the aseismic/seismic transition. *Progress in Earth and Planetary Science*, 5(1):24, December 2018. ISSN 2197-4284. doi:10.1186/s40645-018-0183-8.

[74] Natalia Poiata, Jean-Pierre Vilotte, Nikolai M. Shapiro, Mariano Supino, and Kazushige Obara. Segmentation and interaction of low-frequency earthquake activity along the strike of subducting slab in shikoku, japan. 2020.

[75] William H. Press, Saul A. Teukolsky, William T. Vetterling, and Brian P. Flannery. *Numerical Recipes - The Art of Numerical Computing*. Third edition edition, 2007.

[76] M. Radiguet, F. Cotton, M. Vergnolle, M. Campillo, A. Walpersdorf, N. Cotte, and V. Kostoglodov. Slow slip events and strain accumulation in the Guerrero gap, Mexico. *Journal of Geophysical Research: Solid Earth*, 117(B4), 2012. doi:10.1029/2011JB008801. https://agupubs.onlinelibrary.wiley.com/doi/pdf/10.1029/2011JB008801.

[77] G. Rogers. Episodic Tremor and Slip on the Cascadia Subduction Zone: The Chatter of Silent Slip. *Science*, 300(5627):1942–1943, June 2003. ISSN 0036-8075, 1095-9203. doi:10.1126/science.1084783.

[78] Baptiste Rousset, Roland Bürgmann, and Michel Campillo. Slow slip events in the roots of the San Andreas fault. *Science Advances*, 5(2):eaav3274, February 2019. ISSN 2375-2548. doi:10.1126/sciadv.aav3274.

[79] A. A. Royer, A. M. Thomas, and M. G. Bostock. Tidal modulation and triggering of low-frequency earthquakes in northern Cascadia. *Journal of Geophysical Research: Solid Earth*, 120(1):384–405, January 2015. ISSN 21699313. doi:10.1002/2014JB011430.

[80] J. L. Rubinstein, M. La Rocca, J. E. Vidale, K. C. Creager, and A. G. Wech. Tidal Modulation of Nonvolcanic Tremor. *Science*, 319(5860):186–189, January 2008. ISSN 0036-8075, 1095-9203. doi:10.1126/science.1150558.

[81] Justin L. Rubinstein, Joan Gomberg, John E. Vidale, Aaron G. Wech, Honn Kao, Kenneth C. Creager, and Garry Rogers. Seismic wave triggering of nonvolcanic tremor, episodic tremor and slip, and earthquakes on Vancouver Island. *Journal of Geophysical Research*, 114:B00A01, February 2009. ISSN 0148-0227. doi:10.1029/2008JB005875.

[82] D. M. Saffer. The permeability of active subduction plate boundary faults. *Geofluids*, 15(1-2):193–215, February 2015. ISSN 14688115. doi:10.1111/gfl.12103.

[83] Paul Segall and James R. Rice. Dilatancy, compaction, and slip instability of a fluid-infiltrated fault. *Journal of Geophysical Research: Solid Earth*, 100(B11):22155–22171, 1995. doi:10.1029/95JB02403. https://agupubs.onlinelibrary.wiley.com/doi/pdf/10.1029/95JB02403.

[84] Nikolai M. Shapiro, D.V. Droznin, S.Y. Droznina, S.L. Senuykov, A.A. Gusev, and E.I. Gordeev. Deep and shallow long-period volcanic seismicity linked by fluid-pressure transfer. *Nature Geosci.*, 10:442–445, 2017. doi:10.1038/ngeo2952.

[85] Nikolai M. Shapiro, Michel Campillo, Edouard Kaminski, Jean-Pierre Vilotte, and Claude Jaupart. Low-Frequency Earthquakes and Pore Pressure Transients in Subduction Zones. *Geophysical Research Letters*, 45(20):11,083–11,094, October 2018. ISSN 0094-8276. doi:10.1029/2018GL079893.

[86] David R. Shelly. Complexity of the deep San Andreas Fault zone defined by cascading tremor. *Nature Geoscience*, 8(2):145–151, February 2015. ISSN 1752-0894, 1752-0908. doi:10.1038/ngeo2335.

[87] David R. Shelly, Gregory C. Beroza, Satoshi Ide, and Sho Nakamula. Low-frequency earthquakes in Shikoku, Japan, and their relationship to episodic tremor and slip. *Nature*, 442(7099):188–191, July 2006. ISSN 0028-0836, 1476-4687. doi:10.1038/nature04931.

[88] David R. Shelly, Gregory C. Beroza, and Satoshi Ide. Non-volcanic tremor and low-frequency earthquake swarms. *Nature*, 446(7133):305–307, March 2007. ISSN 0028-0836, 1476-4687. doi:10.1038/nature05666.

[89] Bunichiro Shibazaki and Yoshihisa Iio. On the physical mechanism of silent slip events along the deeper part of the seismogenic zone. *Geophysical Research Letters*, 30(9), 2003. doi:10.1029/2003GL017047. https://agupubs.onlinelibrary.wiley.com/doi/pdf/10.1029/2003GL017047.

[90] R.H. Sibson. Implications of fault-valve behaviour for rupture nucleation and recurrence. *Tectonophysics*, 211(1-4):283–293, September 1992. ISSN 00401951. doi:10.1016/0040-1951(92)90065-E.

[91] T.-R. A. Song, Donald. V. Helmberger, M. R. Brudzinski, R. W. Clayton, P. Davis, X. Perez-Campos, and S. K. Singh. Subducting Slab Ultra-Slow Velocity Layer Coincident with Silent Earthquakes in Southern Mexico. *Science*, 324(5926):502–506, April 2009. ISSN 0036-8075, 1095-9203. doi:10.1126/science.1167595.

[92] M. Supino, N. Poiata, G. Festa, J. P. Vilotte, C. Satriano, and K. Obara. Self-similarity of low-frequency earthquakes. *Scientific Reports*, 10(1):1–9, April 2020. ISSN 2045-2322. doi:10.1038/s41598-020-63584-6.

[93] Stephan Taetz, Timm John, Michael Bröcker, Carl Spandler, and Andreas Stracke. Fast intraslab fluid-flow events linked to pulses of high pore fluid pressure at the subducted plate interface. *Earth and Planetary Science Letters*, 482:33–43, January 2018. ISSN 0012821X. doi:10.1016/j.epsl.2017.10.044.

[94] Yoshiyuki Tanaka, Takehito Suzuki, Yuichi Imanishi, Shuhei Okubo, Xinlin Zhang, Miwako Ando, Atsushi Watanabe, Mamoru Saka, Chiaki Kato, Shuichi Oomori, and Yoshifumi Hiraoka. Temporal gravity anomalies observed in the Tokai area and a possible relationship with slow slips. *Earth, Planets and Space*, 70(1):25, December 2018. ISSN 1880-5981. doi:10.1186/s40623-018-0797-5.

[95] Amanda M. Thomas, Robert M. Nadeau, and Roland Bürgmann. Tremor-tide correlations and near-lithostatic pore pressure on the deep San Andreas fault. *Nature*, 462(7276):1048–1051, December 2009. ISSN 0028-0836, 1476-4687. doi:10.1038/nature08654.

[96] M.P.A. van den Ende, J. Chen, J.-P. Ampuero, and A.R. Niemeijer. A comparison between rate-and-state friction and microphysical models, based on numerical simulations of fault slip. *Tectonophysics*, 733:273–295, May 2018. ISSN 00401951. doi:10.1016/j.tecto.2017.11.040.

[97] Peter E. van Keken, Bradley R. Hacker, Ellen M. Syracuse, and Geoff A. Abers. Subduction factory: 4. Depth-dependent flux of H $_2$ O from subducting slabs worldwide. *Journal of Geophysical Research*, 116(B1), January 2011. ISSN 0148-0227. doi:10.1029/2010JB007922.

[98] Philip E. Wannamaker, Rob L. Evans, Paul A. Bedrosian, Martyn J. Unsworth, Virginie Maris, and R. Shane McGary. Segmentation of plate coupling, fate of subduction fluids, and modes of arc magmatism in Cascadia, inferred from magnetotelluric resistivity. *Geochemistry, Geophysics, Geosystems*, 15(11):4230–4253, November 2014. ISSN 15252027. doi:10.1002/2014GC005509.

[99] E. Warren-Smith, B. Fry, L. Wallace, E. Chon, S. Henrys, A. Sheehan, K. Mochizuki, S. Schwartz, S. Webb, and S. Lebedev. Episodic stress and fluid pressure cycling in subducting oceanic crust during slow slip. *Nature Geoscience*, page 1, May 2019. ISSN 1752-0908. doi:10.1038/s41561-019-0367-x.

[100] Aaron G. Wech and Kenneth C. Creager. A continuum of stress, strength and slip in the Cascadia subduction zone. *Nature Geoscience*, 4(9):624–628, September 2011. ISSN 1752-0894, 1752-0908. doi:10.1038/ngeo1215.

[101] Randolph T. Williams, Peter S. Mozley, Warren D. Sharp, and Laurel B. Goodwin. U-Th Dating of Syntectonic Calcite Veins Reveals the Dynamic Nature of Fracture Cementation and Healing in Faults. *Geophysical Research Letters*, 46(22):12900–12908, November 2019. ISSN 0094-8276, 1944-8007. doi:10.1029/2019GL085403.

[102] Weiqiang Zhu, Kali L. Allison, Eric M. Dunham, and Yuyun Yang. Fault valving and pore pressure evolution in simulations of earthquake sequences and aseismic slip. *Nature Communications*, 11 (1):4833, December 2020. ISSN 2041-1723. doi:10.1038/s41467-020-18598-z.

This work was submitted to Journal of Geophysical Research: Solid Earth (19/02/2021)